NASA/TM—2018–220015

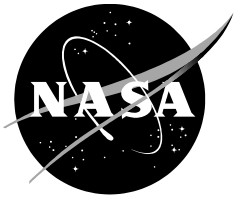

Physical and Biological Properties of Cobalt- and Copper-Doped Calcium Phosphates as Bone Substitute Materials

Haley V. Cummings
Ames Research Center
Moffett Field, California

November 2018

NASA STI Program ... in Profile

Since its founding, NASA has been dedicated to the advancement of aeronautics and space science. The NASA scientific and technical information (STI) program plays a key part in helping NASA maintain this important role.

The NASA STI program operates under the auspices of the Agency Chief Information Officer. It collects, organizes, provides for archiving, and disseminates NASA's STI. The NASA STI program provides access to the NTRS Registered and its public interface, the NASA Technical Reports Server, thus providing one of the largest collections of aeronautical and space science STI in the world. Results are published in both non-NASA channels and by NASA in the NASA STI Report Series, which includes the following report types:

TECHNICAL PUBLICATION. Reports of completed research or a major significant phase of research that present the results of NASA Programs and include extensive data or theoretical analysis. Includes compilations of significant scientific and technical data and information deemed to be of continuing reference value. NASA counterpart of peer-reviewed formal professional papers but has less stringent limitations on manuscript length and extent of graphic presentations.

TECHNICAL MEMORANDUM. Scientific and technical findings that are preliminary or of specialized interest, e.g., quick release reports, working papers, and bibliographies that contain minimal annotation. Does not contain extensive analysis.

CONTRACTOR REPORT. Scientific and technical findings by NASA-sponsored contractors and grantees.

CONFERENCE PUBLICATION. Collected papers from scientific and technical conferences, symposia, seminars, or other meetings sponsored or co-sponsored by NASA.

SPECIAL PUBLICATION. Scientific, technical, or historical information from NASA programs, projects, and missions, often concerned with subjects having substantial public interest.

TECHNICAL TRANSLATION. English-language translations of foreign scientific and technical material pertinent to NASA's mission.

Specialized services also include organizing and publishing research results, distributing specialized research announcements and feeds, providing information desk and personal search support, and enabling data exchange services.

For more information about the NASA STI program, see the following:

Access the NASA STI program home page at http://www.sti.nasa.gov

E-mail your question to help@sti.nasa.gov

Phone the NASA STI Information Desk at 757-864-9658

Write to:
NASA STI Information Desk
Mail Stop 148
NASA Langley Research Center
Hampton, VA 23681-2199

NASA/TM—2018–220015

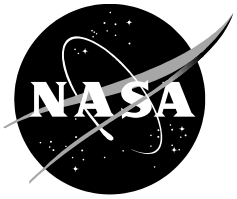

Physical and Biological Properties of Cobalt- and Copper-Doped Calcium Phosphates as Bone Substitute Materials

Haley V. Cummings
Ames Research Center
Moffett Field, California

National Aeronautics and
Space Administration

Ames Research Center
Moffett Field, CA 94035-1000

November 2018

ACKNOWLEDGMENTS

I want to thank Mr. Gregg Westberg of the Microelectronics Research Development Laboratory (MRDL), Dr. Michael Haji-Sheikh of the Northern Illinois University (NIU) Department of Electrical Engineering, Michael Reynolds and Dave Garcia of the NIU Machine Shop, and Stanislaw Kolesnik of the NIU Department of Physics for their assistance and support throughout my research. I would also like to thank Benyamin Salehi, Sarah Fleck, and Kareem Elkwae for working all hours of the night and day to make samples with me. Thanks to Weiguo Han for teaching this mechanical engineer how to work with cells. To my committee, Dr. Federico Sciammarella and Dr. Sherine Elsawa, thank you for your input, support, and patience with me through this research and writing process. Finally, thank you to my advisor, Dr. Sahar Vahabzadeh, for introducing me to your passion in the field of biomaterials and for your recommendations and encouragement through the experimentation and writing of this thesis.

This work is dedicated to my parents, Mike and Melissa, and my brother and sister, Ryan and Lauren, who have shaped me, pushed me, challenged me, and loved me since day one. To my friends, who keep me sane in the insane times, and who ask the tough questions. And to the unexplainable, unattainable God of the universe, in whom science and faith meet, and in the pursuit of whom I find purpose.

TABLE OF CONTENTS

LIST OF FIGURES

LIST OF TABLES

PHYSICAL AND BIOLOGICAL PROPERTIES OF COBALT- AND COPPER-DOPED CALCIUM PHOSPHATES AS BONE SUBSTITUTE MATERIALS

Haley V. Cummings[1]

Ames Research Center

SUMMARY

Arthritis, osteoporosis, and other bone diseases and defects are common medical issues worldwide. By utilizing ceramic biomaterials as bone substitutes to treat these diseases, bone regeneration can be promoted, and toxicity from the substitute material can be limited. Calcium phosphate (CaP) ceramics have become popular as bone substitutes because of their biocompatibility and similarity in composition to natural bone. The purpose of this research was to investigate the physical properties and biological responses of CaP-based bone substitutes, doped with metal ions. Some metal ions are present in natural bone in small amounts, and recent studies show that they affect the biological responses of CaPs significantly. Dopants such as magnesium (Mg), strontium (Sr), silicon (Si), and iron (Fe) alter the phase composition, mechanical properties, and osteogenesis and angiogenesis properties of CaPs, depending on their concentration and method of addition. In the present study, the effects of cobalt (Co) and copper (Cu) on the physical and biological properties of two main CaP materials, brushite cement (BrC) and tricalcium phosphate (TCP), were investigated. Different concentrations of dopants in forms of oxide and/or chloride were selected, and their effects on phase composition, sintering behavior, density, setting time, compressive strength, and *in vitro* interaction with osteosarcoma and osteoblast cells were studied. Different techniques of sample preparation, challenges during cement preparation and compact sample pressing, sintering, and methods of dopant addition are discussed.

The presence of Cu in TCP was found to increase thermal stability of the material and decrease the impact of sintering temperature on porosity. In addition, Cu caused a reduction in expression of inflammatory gene markers by human osteoblast cells and an increased expression at early time points of osteoinductive markers.

The addition of Cu and Co to brushite cement caused an increase in thermal stability of the material, and the addition of Cu caused a significant increase in setting time. Small dopant amounts of Co caused a decrease in setting time, but higher amounts caused an increase. In addition, Cu dopant in small amounts resulted in an increase of compressive strength. Both Cu and Co led to a decrease in expression of inflammatory gene markers by osteoblast and osteosarcoma cells, respectively, and Cu also caused an increase in osteoinductive marker expression. These results indicate that Cu and Co have a positive impact on the physical, mechanical, and biological properties of CaP biomaterials.

[1] Thesis submitted to Dr. Sahar Vahabzadeh, Director, Northern Illinois University, Department of Mechanical Engineering, De Kalb, Illinois, May 2018, in partial fulfillment of the requirements for the degree of Master of Science.

CHAPTER 1 INTRODUCTION

1.1 Biology of Bone

The dry bone mass of a healthy adult comprises 15–20% of his/her total body weight while the skeletal system overall constitutes 30–40% of an adult's weight [1]. This system is integral in structurally supporting the body and protecting the vital organs, and it also enables motion through connection with the muscles. What is often referred to as "bone" is more formally known as osseous tissue. The two types of bone tissue present in the body and depicted in Figure 1 [2] are cancellous and cortical, which are mainly identified by their densities. Cortical bone is much denser than cancellous bone; cancellous bone is porous, flexible, and much weaker than cortical. At the microstructure level, cortical bone functions through the Haversian, or osteon, system. In this system, the blood flow is conducted through "Haversian canals," which are in the middle of each osteon and are surrounded by a cylindrical lamellae tissue layer made from collagen fibers [2]. These single Haversian systems are reported to have tensile strengths of around 17 ksi, compressive strengths around 16 ksi, bending strength around 56 ksi, and torsional strength around 29 ksi [3–6]. In contrast, cancellous bone (see Table 1) is composed of trabecula, which is bone tissue formed into a rod to enhance mechanical functionality. This structure allows cancellous bone to have a higher degree of porosity, mostly greater than 75%, while still maintaining a reasonable strength, depending of course on the age of the bone and region in the body [8,9].

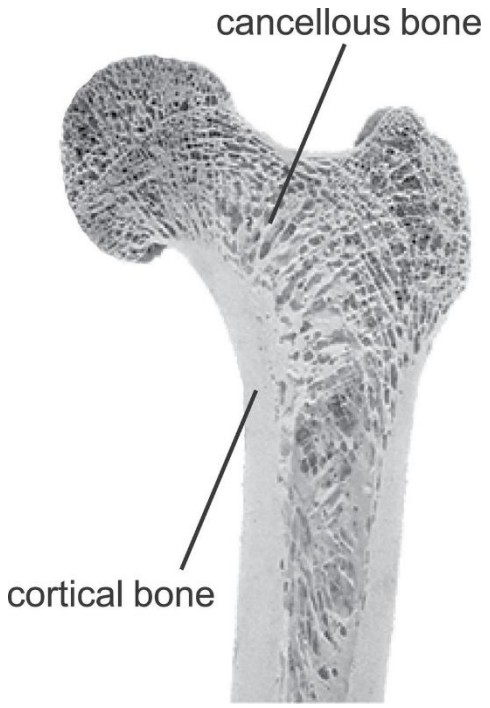

Figure 1. Cortical bone vs. cancellous bone [7].

Table 1. Properties of cancellous bone [8].

Mechanical Property	No. of Samples	Age	Apparent Density (lb/in^3)
Young's Modulus (Mpa)	142	67 ±15	0.00978
Shear Modulus (Mpa)	42	Bovine	–
σ_y (MPa, tension)	52	65 ±14	0.01048
σ_y (MPa, compression)	68	65 ±14	0.00978 ±0.00614
σ_{ult} (MPa, tension)	22	54 ±11	0.00686 ±0.00145
σ_{ult} (MPa, compression)	22	54 ±11	0.00614 ±0.00145

Cortical bone is often found as the outside tissue surrounding the inner cancellous bone, though cancellous bone is also found on the end of longer bones such as the femur. Mechanical properties of the femur, tibia, and other bones are shown in Table 2. Cancellous bone is remodeled more often than cortical bone; this is a function of its higher metabolic activity compared to cortical bone, and it also means that it is often younger than cortical bone [2]. This remodeling process involves the resorption of old bone tissue and the formation of new bone tissue and occurs mainly as a function of the bone cells. Osteoblasts are the bone-forming cells but they are also involved in resorption, while osteoclasts only perform the resorption. When osteoblasts form new bone, it is initially uncalcified and known as osteoid bone.

Table 2. Properties of human bone [10].

Human (20–39 years) Bone	Femur	Tibia	Humerus	Radius
Ultimate Tensile Strength (Mpa)	124 ±1.1	174 ±1.2	125 ±0.8	152 ±1.4
Ultimate Percent Elongation	1.41	1.50	1.43	1.50
Modulus of Elasticity in Tension (Gpa)	17.60	18.40	17.50	18.90
Ultimate Compressive Strength (Mpa)	107 ±4.3			
Ultimate Percentage Contraction	1.85 ±0.84			
Ultimate Shear Strength (Mpa)	54 ±0.6			
Torsional Modulus of Elasticity (Gpa)	3.20			

Osteoblasts originate from mesenchymal stem cells (MSCs), which are multipotent cells that have the potential to differentiate into osteoblasts, adipocytes, chondrocytes, and myoblasts [11]. MSCs that differentiate to osteoblasts react to the runt-related transcription factor 2 (RUNX2) protein, and osteoblast differentiation, in turn, is regulated by various hormones as shown in Figure 2 [12,13]. Osteoblasts differentiate into bone lining cells known as osteocytes [14]. These osteocytes embed themselves in the bone matrix newly formed by osteoblasts and may also play a role in mechanical stress transduction and thus gene regulation, though this process is not yet well understood [15–17]. The continued differentiation of osteoblasts relies on osteoblast-produced cytokines like insulin growth factor 1 (IGF-1) and bone morphogenetic proteins (BMPs) [11]. Collagen, which makes up a significant portion of the organic portion of the bone matrix, is produced by osteoblasts, as are noncollagenous proteins like osteocalcin and osteonectin [11].

Another significant protein secreted by osteoblasts is osteoprotegerin (OPG), which is a decoy receptor for receptor activator of nuclear factor kappa-ß ligand (RANKL). This is significant because differentiation of osteoclasts relies on RANKL binding with receptor activator of nuclear factor κ ß (RANK) [19,20]. Thus, as OPG binds with RANKL instead, osteoclast differentiation is inhibited (Figure 3).

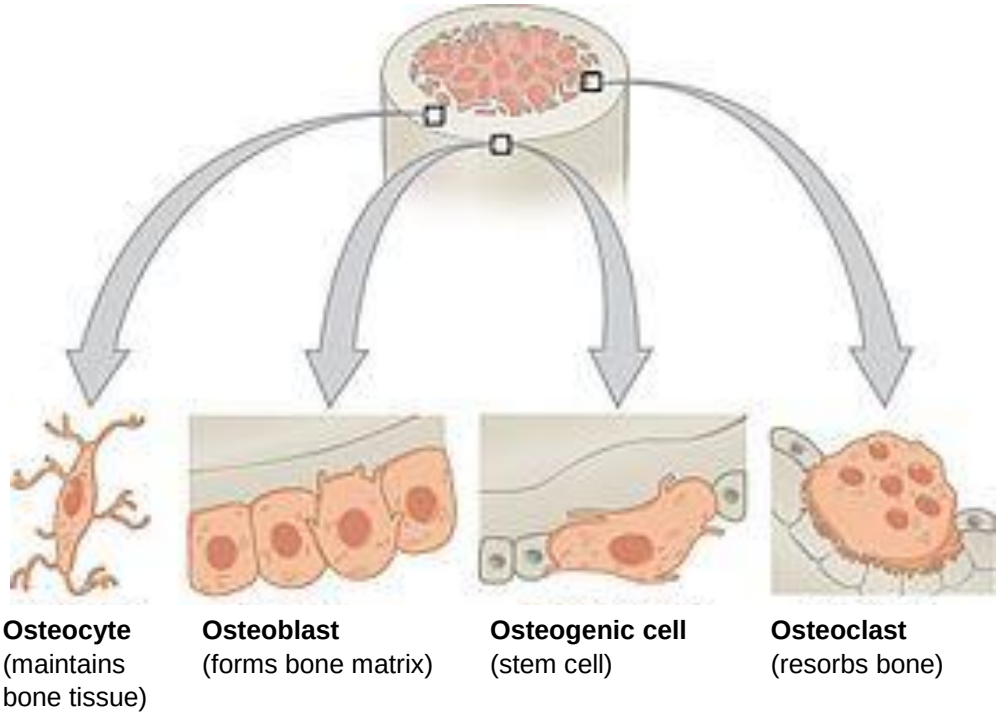

Figure 2. Constant bone remodeling process facilitated by osteoclasts and osteoblasts [18].

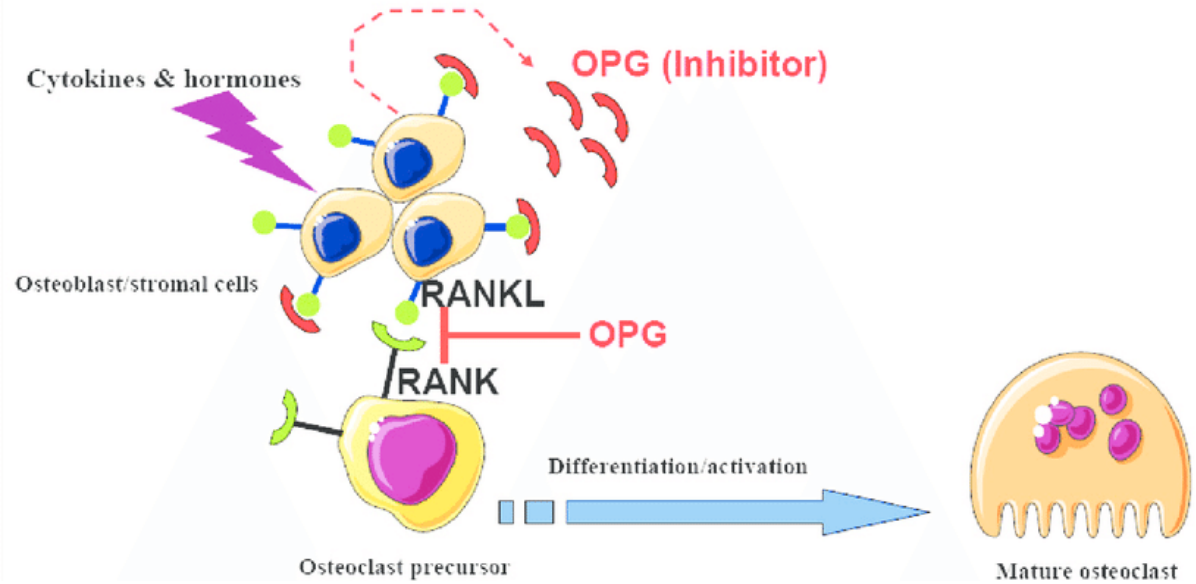

Figure 3. RANKL binding mechanism [21].

Compared to osteoblasts, osteoclasts are large, multinucleated cells whose main purpose is the resorption of bone. To resorb bone, osteoclasts attach to the surface of the bone and create a seal around the area to be resorbed. They then secrete hydrochloric acid, which dissolves the mineral, and the proteolytic enzyme cathepsin K, which breaks down the bone matrix [19,22]. As mentioned previously, the differentiation of osteoclasts is significantly regulated by the prevalence of OPG, RANKL, and RANK, where an overabundance of OPG can cause the resorption process to decrease, leading to increased bone mass and thus osteopetrosis, and conversely a lack of OPG can lead to excessive bone resorption and osteoporosis [23]. However, there are many other markers that indicate healthy bone formation, including alkaline phosphatase 1 (ALP-1), vascular endothelial growth factor (VEGF), interleukin-6 (IL-6), interleukin-17 (IL-17), tumor necrosis factor-α (TNF-α), collagen type 1 α (COLA-1), osteocalcin (OCN), and hypoxia inducible factor 1-α (HIF-1α).

1.2 Effective Markers in Bone Remodeling

OPG and RANKL—As previously discussed, OPG is a decoy receptor for RANKL secreted by osteoblasts. It has been observed that with an upregulation of RANKL, OPG is downregulated and osteoporosis results [19]. However, when OPG is able to bind with RANKL, osteoclostogenesis is inhibited [24]. Studies have shown that OPG-deficient mice experience osteoporosis and loss of bone mass while OPG-transgenic mice experience osteopetrosis [25]. Interestingly, OPG has also been observed to inhibit calcification of large blood vessels [19]. RANKL is a member of the tumor necrosis factor (TNF) family, and its expression is affected by T cell activation [24]. It plays a major role in the formation and activation of osteoclast cells and also appears to play a role in rheumatoid arthritis joint breakdown [19].

ALP—ALP is an osteoblast-synthesized ectoenzyme that plays a role in bone calcification [26–28]. Its exact role is not fully understood, but it is clearly linked to healthy bone. An increased expression of ALP is observed with osteoblast differentiation, and many studies suggest that early indication of cellular activity and differentiation can be gathered from the measured ALP expression [29]. In addition, mechanical force has been observed to increase ALP expression, and ALP expression is increased during fracture healing [28].

VEGF—This growth factor is expressed by osteoblasts, osteoclasts, and chondrocytes, and it stimulates and regulates their growth, differentiation, proliferation, and survival [30–32]. It also plays a large role in angiogenesis, or the growth of blood vessels, as well as in the ossification of bone [33,34]. Osteogenesis and angiogenesis are closely related and interdependent, and VEGF is one growth factor that bridges the gap between the two. VEGF is integral in endochondral ossification, which is one method by which bone is ossified [30]. VEGF has been found to stimulate osteoblast differentiation by as much as 70%, though low expression is observed at the beginning of osteoblast differentiation, and most expression of VEGF occurs during mineralization [35,36]. Several studies have shown that scaffolds incorporated with VEGF and slow-release mechanisms are therapeutic for bone healing [30,37]. However, excessive amounts of VEGF can also decrease bone healing [31].

IL-6—The presence of the proinflammatory cytokine IL-6 can stimulate bone formation by inducing osteoblast differentiation and can also inhibit the formation of osteoclasts [38,39]. It also enhances the formation of the extracellular matrix (ECM) and increases expression of ALP< OCN and other genes that are involved in calcification [39,40]. An increased presence of IL-6 has been found in the joints of patients with osteoarthritis, and inhibited expression of IL-6 has been found to eliminate osteoarthritis in mice studies [38,41]. In addition, osteoblasts have seen protection from apoptosis because of TNF-α serum depletion by IL-6, though results are inconclusive [39].

IL-17—The IL-17 cytokine is proinflammatory and mostly originates from specialized T cells [42,43]. It is associated with inflammatory diseases like rheumatoid arthritis and is profuse in the sunovial fluid of such patients' joints. Studies have shown IL-17 to stimulate ALP expression in MSCs and to have a positive effect on calcium and mineralized deposition of the ECM [44]. Reports also show that IL-17 promotes osteogenesis and osteoclastogenesis, though its role is still being defined [43,44]. IL-17 may have a stimulating effect on RANKL expression and also may promote osteogenic differentiation of MSCs [43,45].

TNF-α—The TNF-α cytokine is mainly secreted by macrophages and leads to the formation and activation of osteoclasts [46]. It is also linked to reduced osteoblast proliferation, and it has been found to limit the expression of differentiation markers of osteoblasts like OCN, COLA-1, and ALP. As such, TNF-α is associated with bone loss and excessive bone resorption and is associated with inflammatory bone diseases [46]. In rat calvaria models, the addition of TNF-α decreased the osteoblast proliferation to maturity and decreased osteoblast differentiation [47].

COLA-1—Collagen is abundantly produced by osteoblast cells, and COLA-1 is a gene that produces part of type 1 collagen, which is completed by the chain produced by COLA-2. Type 1 collagen is fibril forming and is essential to the production of the ECM [48]. In addition, the COLA-1 gene has been linked to ALP production and the differentiation of osteoblast cells [48].

OCN—Osteocalcin is secreted almost entirely by osteoblast cells and is one of the most prolific noncollagenous proteins found in bone [49,50]. Secretion of this protein is found mostly in mature osteoblast cells, and it acts to recruit osteoclasts and osteoblasts [51]. It also plays a role in signaling and is considered an indicator of bone formation [49–51]. OCN's ability to bind with hydroxyapatite makes it an integral part in the mineralization of bone and the ECM, though some studies suggest that OCN does not play a role in bone mineralization [50–52]. OCN is also an indicator of bone metabolic activity [49].

HIF-1α—In general, the activation of hypoxia inducible factors (HIFs) occurs in response to a reduction in oxygen, as the name suggests. HIF-1α specifically encodes the α subunit of HIF-1 and activates the transcription of genes such as VEGF. As such, HIF-1α is a crucial link between angiogenesis and osteogenesis in skeletal and bone formation [53,54]. In addition, studies show that a lack of HIF-1α results in bones with a smaller diameter and a lack of vascularization, and that HIF-1α contributes to the protection of articular cartilage in certain cases [53,55].

1.3 Need for Bone Substitute Materials

Osteoporosis, arthritis, bone fracture, and other bone trauma are prevalent around the world and cause significant loss of productivity and decrease in quality of life. According to a 2017 Centers for Disease Control study, the 10-year probability of a hip fracture within the next 10 years for an individual aged 80 or older in the United States is 72% [56]. This fracture becomes more likely with osteoporosis because, as shown in Figure 4, the density of bone decreases. In addition, it is estimated that 16% of Americans suffer from arthritis, and 43% of those experience physical limitations due to the disease [57]. In 2013, arthritis cost $304 billion in wages lost and medical expenses incurred [58]. In addition, astronauts exposed to prolonged zero-gravity effects experience greater risk for osteoporosis and bone loss, especially in the spine or hip [59].

Figure 4. Imbalance of osteoclast and osteoblast activity leads to osteoporosis [60].

Established methods such as grafts (Figure 5) have been implemented in the medical community to alleviate the effects of bone loss. Autografts, which are tissue grafts from one place on a patient's body to another, are by far the desired remedy, but this solution requires two surgeries and additional time under anesthesia for the afflicted individual, which increases the potential for additional damage. Allografts are tissue grafts from a donor to a patient and are another viable solution, but the patient's body may reject the donated tissue. An allograft from a genetically identical donor is known as a synograft and is usually not rejected by the patient's body, but this method of transplant still requires two surgeries. Transplanting tissue from a different species, known as a xenograft, is also utilized in the medical industry but, as with allografts, there is a potential for the body to reject the unknown tissue.

As an alternative solution, much emphasis has been placed on biomaterials. In a general sense, a biomaterial is any synthetic or natural material that is used in the body, and can include metals, ceramics, polymers, and any combination of these.

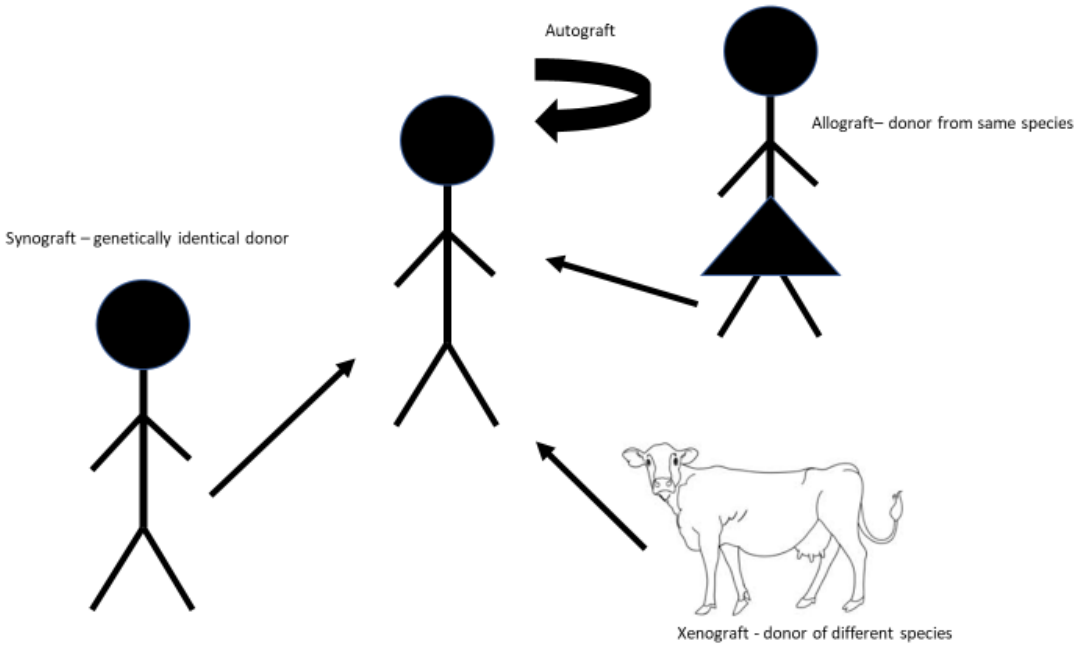

Figure 5. Types of grafts.

Heat-activated polymers are particularly intriguing as drug delivery systems and stents. For load-bearing bone sections or joint replacement, metal biomaterials are a natural choice because they are strong and resistant to fatigue. However, metals are often toxic to the body and, as they remain in the body over time, tend to leach harmful ions into the body. This can cause significant health concerns, as observed with metal-on-metal hip prostheses that require a second surgery to remedy the issues [61]. In addition, these materials do not integrate with the surrounding bone, which can cause a phenomenon known as fibrous encapsulation (Figure 6) that occurs when the implant is surrounded by tissue but not integrated into the body [62]. This can cause the implant to loosen and eventually can necessitate a second surgery to repair the affected area. To counter this, the metal can be coated with a ceramic material. Ceramics have a composition like that of bone, which allows the body to more readily accept the implant and integrate it into the body. In addition, the coating can reduce the toxicity of the implant by eliminating the friction between the implant and the surrounding bone.

However, in small bone defect sites in non-load-bearing areas, ceramics are often viewed as superior to metals. While these materials lack tensile and fracture strength, they have excellent compressive strength and, as previously mentioned, have similar composition to natural bone. There are numerous varieties of ceramics available and effective as implants, including bioglasses, metal oxides, and calcium phosphates.

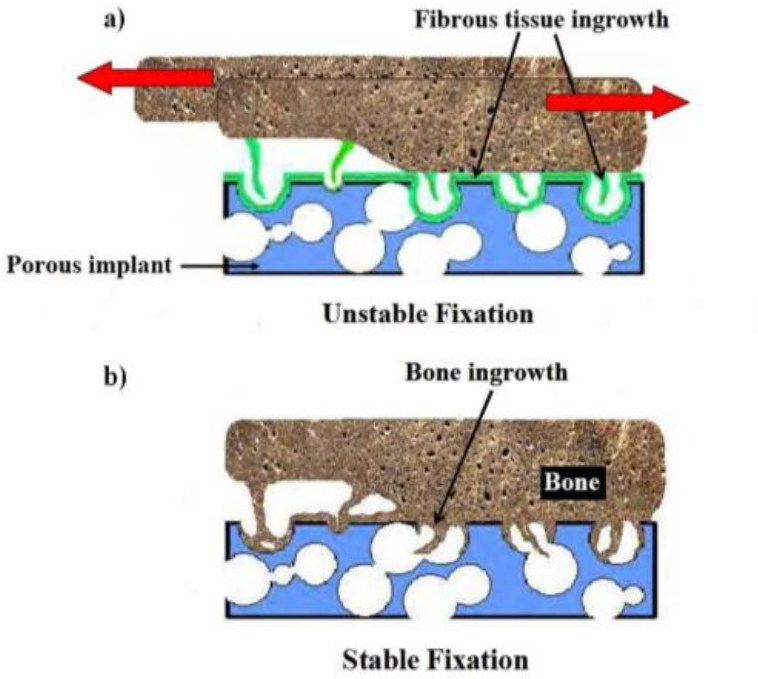

Figure 6. Fibrous encapsulation vs. stable fixation [63].

Bioceramics are advantageous for use in biomaterial applications because they are often not toxic to the body. Some bioceramics, when implanted, can bond with the surrounding tissue and thus have superior fixation compared to metals or other inert ceramics. Some ceramics are inert and experience fibrous encapsulation, but this can be avoided if the material is porous. The porosity of many ceramics can be manipulated and optimized to ensure adequate pore size and distribution. Both macroporosity (>100 μm) and microporosity (<100 μm) are desired in biomaterials for biodegradability, fixation, and enhanced osteoconduction [64]. If a material has surface reactivity with the surrounding tissue, it will biologically fixate to the tissue and avoid detrimental fibrous encapsulation. Porosity plays a large role in accomplishing this and is necessary for the circulation of blood and new cells while also providing a mechanism for waste removal. Growth factors, BMPs, and other osteogenic factors also circulate through these interconnected pores and ultimately lead to enhanced osteoinduction. Mechanical strength is also regulated through pore size and interconnectedness. Thus, CaP biomaterial porosity is an integral consideration in designing scaffolds and implants.

1.4 Calcium Phosphate Bone Substitutes

CaP ceramics are well-suited for bone substitution applications, as their composition is similar to that of human bone. Bone is composed of 36 wt. % calcium and 17 wt. % phosphorous (Table 3), which allows the body to more readily accept these ceramic bone substitutes compared to other materials that the body is unfamiliar with and thus rejects [65]. In addition, because of the similarity of the material to bone, CaPs often elicits a biological response from the body and bonds are formed between the implant and the native bone tissue. This leads to greater integration and higher success levels of implants. CaPs are also resorbable, which means the implant dissolves as the bone tissue regenerates. The physiological reactions of the many types of CaPs are distinguishable by their calcium-to-phosphate (Ca/P) ratio, which can be used to determine the solubility product and thus the application of the material, as well as by their phase composition and crystallinity. CaPs with a small solubility product such as hydroxyapatite (HA) have a high Ca/P ratio and are useful for more permanent applications, as the substitute will dissolve slowly over many years [66]. In contrast, materials with high solubility products and low Ca/P ratios, such as monocalcium phosphate monohydrate (MCPM), dissolve quickly and are useful in short-term applications [66]. Tricalcium phosphate (TCP) and dicalcium phosphate dihydrate (DCPD), which is also known as brushite, are of specific interest in this research. TCP can be expressed in two different phases (Table 4) based on the temperature at which it is calcined: α-TCP, which forms at temperatures above 1250 °C, and ß-TCP, which forms at lower temperatures and is stable up to 1125 °C [67]. α-TCP has a solubility factor of 10^{-26} while ß-TCP has a solubility factor of 10^{-29}, though both phases have a Ca/P ratio of 1.5 [66]. This difference in solubility products by a factor of 3 is significant and is a good example of how minor variations in Ca/P ratio can affect the solubility product. The Ca/P ratio of DCPD is 1.0, and it has a solubility factor of 10^{-7}, which indicates a much higher rate of resorbability compared to TCP [66]. DCPD is often used as a cement because of its high solubility product. However, as ceramics, these materials have low tensile and fracture strengths, which makes them unsuitable substitutes in load-bearing areas, though they can be used in small defects that bear relatively small loads [68]. In addition, as the implants are resorbed, their mechanical strength will decrease because of the dissolution of the material.

Table 3. Composition of bone relative to mineral fraction or wet human bone (cobalt and copper) [69,70].

Wt. %	Bone (%)
Ca	36.6
P	17.1
CO_2	4.8
Na	1
K	0.07
Mg	0.6
Sr	0.05
Cl	0.1
F	0.1

Table 4. Calcium phosphate biomaterials [66].

Calcium Phosphate	**Abbreviation**	**Chemical Formula**	**Ca/P Molar Ratio**	**Solubility Product**
Monocalcium phosphate monohydrate	MCPM	$CaH_4P_2O_8$	0.5	7.2×10^{-2}
Dicalcium phosphate dihydrate (brushite)	DCPD	$CaHPO_4\ 2H_2O$	1	2.5×10^{-7}
α-tricalcium phosphate	α-TCP	$\alpha\text{-}Ca_3(PO_4)_2$	1.5	3.16×10^{-26}
β-tricalcium phosphate	β-TCP	$\beta\text{-}Ca_3(PO_4)_2$	1.5	1.25×10^{-9}
Hydroxyapatite	HA	$Ca_5(PO_4)_3(OH)$	1.67	1×10^{-38}

1.5 Osteoinductivity of Biomaterials

To quantify the performance of these bone substitute materials, the osteoconductivity and osteoinductivity of the materials are observed, among other properties. Osteoconductivity, which is the ability of a material to act as a scaffold for new bone growth, is an inherent property of all CaPs. Osteoinductivity, which is the ability of a material to induce new bone formation without growth factors, is a property that CaPs without additives do not possess. In specific instances, some CaPs have exhibited osteoinductive properties, but the enhancement of the osteoinductive properties of CaPs remains a crucial topic in bone engineering [71]. Osteoinduction is vital because these CaP bone substitutes should contribute to the ultimate healing of the defect site. As previously mentioned, as the substitutes are resorbed, new bone formation should occur so that the defect site can return to complete functionality.

Several methods for enhancing osteoinduction have been studied and reported, including using CaPs enhanced with trace amounts of metal ions or growth factors [68,72–74]. The use of growth factors to enhance osteoinductivity has been well documented, and many studies using bone morphogenetic proteins (BMPs), insulin-like growth factors (IGFs), MSCs, vascular endothelial growth factors (VEGFs), and others can be found [75–78]. These growth factors enhance cell proliferation and the expression of many proteins and indicators of bone growth such as collagen and osteocalcin. Likewise, there is a wealth of research and publications regarding incorporation of metal ions into CaPs to enhance osteoinductivity. Trace elements are found in small amounts within the body already, and they play vital roles in maintaining health. Iron's presence in the blood, magnesium's presence in tissue, and zinc's cellular presence are just a few examples. By incorporating trace amounts of metal in CaP bone substitutes, the therapeutic effects of these metals can be harnessed. Of course, an excess of metal is toxic at the cellular level, and as such, in-depth studies must be conducted. Mg, Li, Fe, Si, Sr, Cu, Co, Zn, and many others are among the elements have been studied. Depending on the amount of trace element used, the type of CaP, the type of cell or implant location studied, and other factors, the biological response varies. Zn and Sr are often utilized or combined in cellular studies. They have been found to increase ALP expression and cell adherence in osteoblast cells cultured on doped BrC samples, as well as in pig trabecular bone [79]. Other studies have corroborated the positive effects of doping CaPs with Zn and Sr on bone formation and healing [76,80]. Mg has also been linked to OPG and RANKL levels and bone morphogenic protein 2 (BMP-2) expression [81–83]. Cell differentiation and proliferation have been enhanced with the incorporation of Li as a dopant in CaP materials, as has the ability of the cell structure to mature [84–86]. Si promotes expression of VEGF and ALP and also enhances matrix mineralization through collagen production [87–90]. In this current research, Cu and Co specifically were studied and were observed as dopants in both ß-TCP and BrC in various dopant amounts.

1.6 Trace Elements Used to Enhance Osteoinductivity

Instances of both cupric (Cu^{2+}) and cuprous (Cu^{+}) copper can be found in the body; most copper intake comes from digested food, while about 10% comes from water [91]. A normal adult has between 18–45 µg of Cu per gram of dry weight located within the liver and about 6 mg of Cu in the blood [92]. Copper plays a strong role in Fe metabolism and is itself metabolized in the liver and absorbed mostly in the small intestine, where it is bound to albumin and transported in blood [91,93]. For the average adult, a lethal dose of Cu is between 10–20 grams, while general Cu toxicity can lead to liver cirrhosis. In cellular toxicity, the most popular theory states that cell death occurs because of the free ions of Cu forming reactive oxygen species (ROS) [91]. Regarding cellular presence, Cu has been linked to angiogenesis, or the growth of blood vessels, and to the expression of VEGF, which is a vital growth factor that is expressed during angiogenesis [94–96].

Cobalt is another essential element that is well known in the composition of vitamin B_{12}. The highest concentrations of Co are found in the liver and kidney, while it is absorbed from the gastrointestinal and pulmonary tracts [97]. The average adult has an intake between 5–45 µg of Co per day and has about 1.5 mg of Co stored in the body [97,98]. It has been reported that the main source of Co toxicity comes from essential macromolecules mistakenly binding to Co instead of the correct element. This causes the macromolecule to function improperly and is most common for macromolecules seeking Fe because of the similar radius of Fe and Co [99]. In clinical settings, the administration of Co was used for treatment of anemia in the 1940s, where 18.5–37 mg Co per day was prescribed to patients. These patients did not show any significant signs of toxicity, but children given 3–4 mg of cobalt chloride per kg of body weight experienced goitrogenic effects until the dose was discontinued [98]. In addition, cardiomyopathy outbreaks were reported from those who ingested Co-infused beer, and neurological symptoms were experienced because of Co toxicity from metal-on-metal hip prostheses [97,100,101].

1.7 Fabrication of Bone Substitute Materials

Fabrication methods of CaP bone substitute materials are diverse and depend extensively on their application and the desired properties. 3D printing of bioceramics offers the fabricator the ability to design scaffolds with specific pore size and overall shape and allows quick reproduction. In addition, growth factors and proteins can easily be incorporated into the scaffold. To incorporate these biological factors, however, low-temperature printing is needed, which poses a challenge [102]. The integration of polymers into the scaffold to enhance the mechanical properties and reduce material impurities has also been utilized in the form of particle leaching, thermally induced phase separation, electrospun scaffolds, and others [103,104]. The aforementioned methods allow for customizable pore size and enhanced interconnectivity of the materials. Other applications require injectability, for which cements are particularly well suited. Cements are created by mixing a solid and a liquid, after which their shape can be molded before the setting reaction completes and the cement is hardened. In addition, these cements inherently have microporosity, which enhances biointegration [105]. Early issues observed with the use of cements were poor binding properties, so additives such as polyethylene glycol (PEG) were necessary to eliminate such problems [106,107]. To fabricate, the powder and liquid are mixed,

poured into a mold, and allowed to set at high humidity. Other methods of powder preparation include uniaxial and isostatic pressing followed by sintering at high temperatures [108].

1.8 Research Objectives

Based on the literature review and previous research conducted, new areas of research were defined. The prevalence of CaPs used as biomaterials is evident, but much research and discovery are yet to be done before these ceramics can reach their potential for impacting the medical community.

The biocompatibility, resorbability, mechanical properties, physical properties, and manufacturability exhibited by TCP and DCPD contributed to the decision to utilize these as the two materials investigated herein. Significant previous research has been done regarding these materials, and this research serves to extend that knowledge base.

Cu has been identified as an essential trace element in living tissue, and previous studies have shown its effectiveness in stimulating angiogenesis and cell proliferation. The research lacks details regarding the effect of Cu on specific markers of osteoinductive genes, and lacks coverage of Cu additives in brushite cement and TCP samples.

Likewise, the anti-inflammatory effects of Co additives to bioceramics have been documented, but Co as an additive to brushite as a scaffold for cell growth is relatively absent in literature, as are studies discussing the role of Co in cell proliferation.

Thus, the research objectives of this study are:

1. Quantify the physical, mechanical, and biological effects of doping TCP with Cu.

TCP powder was synthesized by the solid-state method, and relative amounts of Cu were added prior to calcination at 1050 °C. The resulting powder was mixed with ethanol and ball-milled to break up the material into fine powder, and then dried in a furnace. Fine powder was formed into cylinder scaffolds by a die and uniaxial press and subsequently sintered. The crystal structure of the samples was studied by x-ray diffraction (XRD), and the surface morphology was observed by scanning electron microscopy (SEM). The density was tested by measuring volume, dry and wet weight of samples, and using Archimede's method of calculation. For biological studies, the samples were sterilized and then seeded with osteoblast cells, which were harvested at various time points. Quantitative real-time polymerase chain reaction (qPCR) methods were used to quantify gene expression, and XTT assay was used to obtain cellular proliferation.

2. Quantify the physical, mechanical, and biological effects of doping BrC with Cu and Co.

Brushite powder was obtained by first synthesizing TCP powder and calcinating at 1050 °C. To obtain fine powder, the calcinated material was mixed with ethanol, ball-milled, and dried in a furnace. Half of the powder was kept coarse, and a mixture of fine TCP, coarse TCP, monocalcium phosphate monohydrate (MCPM), magnesium hydrogen phosphate trihydrate, sodium pyrophosphate dibasic, and magnesium sulphate was ground with a mortar and pestle to mix evenly. XRD was used to quantify crystal structure, and SEM illuminated the surface

morphology. Compression testing was conducted to obtain the compression strength, and a Gilmore needle was used to test setting time. The brushite powder was mixed with a polyethylene glycol (PEG)-water combination to form cement and then poured into a mold. Samples were allowed to set at 100% humidity for 1 hour, then submerged in phosphate-buffered saline (PBS) for 24 hours to complete setting reaction. Sterilized samples were seeded with osteoblast cells, and qPCR and XTT assay were used to obtain gene expression and cell proliferation.

CHAPTER 2 COPPER-DOPED TCP

2.1 Introduction

While all CaPs are osteoconductive, many of them, including β-TCP, lack osteoinductivity [73]. Osteoinduction in CaPs including ß-TCP is often enhanced by incorporating growth factors and dopants [68,72,73]. The effects of bone morphogenic protein 2 (BMP-2) addition to gelatinous ß-TCP scaffolds were studied *in vivo* in the back subcutis of rats, and it was found that with increased percentage of BMP-2 incorporation into the scaffolds, increased alkaline phosphatase (ALP) and osteocalcin (OCN) activity was observed, and thus osteoinductivity was enhanced [75]. This study also found that the phase intensity of ß-TCP increased with increasing Co [109]. In another study, β-TCP doped with MgO, SrO, and SiO_2 was substituted into distal femur cortical defect in rats, and histomorphology of the defects was performed 4, 8, 12, and 16 weeks post-implantation [110]. The physical properties of the samples were affected by the dopants, as the XRD results showed the β-to-α transition temperature increased as a result of MgO addition. Further, β-TCP doped with a combination of MgO and SrO was found to enhance bone formation and remodeling through high osseous activity [110]. Previously it was shown that osteoblast cells cultured in the presence of Li-doped β-TCP had increased cell adhesion and proliferation compared to pure TCP samples [84]. The stability of the Li-doped samples was also increased, as was the bulk density of the samples because of the decrease of lattice volume by substitution of Li ions into the Ca sites [84].

Cu has been widely used in biomedical applications and is necessary for many physiological processes and for certain intracellular protein functions [111,112]. The average 70-kg adult male contains approximately 100 mg of Cu, with the highest concentration distributed within the liver, and Linder also reports an average of 1.11 μg/ml of Cu in both whole blood and in plasma [113]. Further, Cu-deficient anemia can result in skeletal deformities, and Cu deficiency is linked to defective tissue formation [114]. Cu deficiencies also affect the metabolism of other trace elements; for example, it increases the iron (Fe) concentration in the liver significantly [115]. In addition, Cu metabolism is affected by inflammation and infection [93]. Many studies have shown improved angiogenesis in Cu-substituted biomaterials while no adverse effect on cellular response was reported. Wu et al. found increased vascular endothelial growth factor (VEGF) and stabilized hypoxia-inducible factor 1-alpha (HIF-1α) expression in Cu-doped bioglass scaffolds, whereas no adverse effect on mesenchymal stem cell proliferation was found because of the presence of Cu [116]. Enhanced angiogenesis was also found in Cu-loaded dicalcium phosphate dihydrate (DCPD) scaffolds at 56- and 560-ng Cu loading when implanted into the peritoneal cavity of mice [95]. Ewald et al. showed that not only the angiogenic properties, but also the

osteoblastic proliferation and activity, were enhanced in DCPD when loaded with 5.65 and 0.56 $\mu g/cm^2$ Cu [117]. In this work, the experiments focused on elucidating the effects of different concentrations of Cu on the proliferation and differentiation of osteoblasts in ß-TCP. Markers of differentiation and inflammation including OPG, COLA-1, ALP-1, OCN, VEGF, IL-6, TNF-α, and RANKL were investigated

This study hypothesized that the addition of Cu to ß-TCP in trace amounts will alter osteoblast (OB) cell growth and gene expression, and sample phase composition and microstructure. To validate, corresponding amounts of CuO were added to TCP precursors, and samples were prepared by uniaxial press and sintering. OB cells were seeded and allowed to grow before harvesting and analysis by XTT and quantitative real-time polymerase reaction (qPCR). X-ray diffraction (XRD) and scanning electron microscopy (SEM) were also utilized to analyze the phase and microstructure of samples.

2.2 Materials and Methods

2.2.1 Sample Preparation

Pure TCP powder was prepared by solid-state synthesis, explained in detail in reference [106]. Briefly, two moles calcium hydrogen phosphate anhydrous ($CaHPO_4$, Alfa Aesar, >99.0%) and one mole calcium carbonate ($CaCO_3$, Alfa Aesar, >98.0%) were ball-milled at a powder:milling media ratio of 1:4 for 2 hours and then calcined at 1050 °C for 24 hours in a muffle furnace. The calcined powder was naturally cooled to room temperature. Copper (II) oxide was added to $CaHPO_4$ and $CaCO_3$ precursors at 0.25, 0.5, and 1.0 wt. % concentrations to prepare the doped TCP, and the mixture was processed similar to undoped TCP. Hereinafter, these concentrations are referred to as Pure-TCP, 0.25 Cu-TCP, 0.5 Cu-TCP, and 1.0 Cu-TCP. The powder was then crushed and mixed with ethanol for 6 hours at a powder:ethanol ratio:milling media ratio of 1:1.5:5. The mixture was then dried at 65 °C for 3–4 days, until all the ethanol was evaporated. Powder was poured into a 13-mm-diameter die set, which was held at 25.5 kN for 2 minutes by a uniaxial press. Samples were then transferred to a porous zirconia substrate and sintered at 1150 °C for 2 hours using a muffle furnace, followed by cooling to room temperature.

One issue that was discovered during the sample preparation was that the surface of all the samples was shearing off after the die was compressed with the uniaxial press. This problem was mitigated by preparing two samples at the same time in the die. The first sample always sheared and broke apart, but the second sample had no surface cracks or blemishes. This was due to the length of the pin in the die set. According to the die manufacturer, the correct range of material powder must be added to the die in order to produce desirable samples, like those in Figure 7. In order to obtain the desired sample dimensions, the two-sample method described above was used.

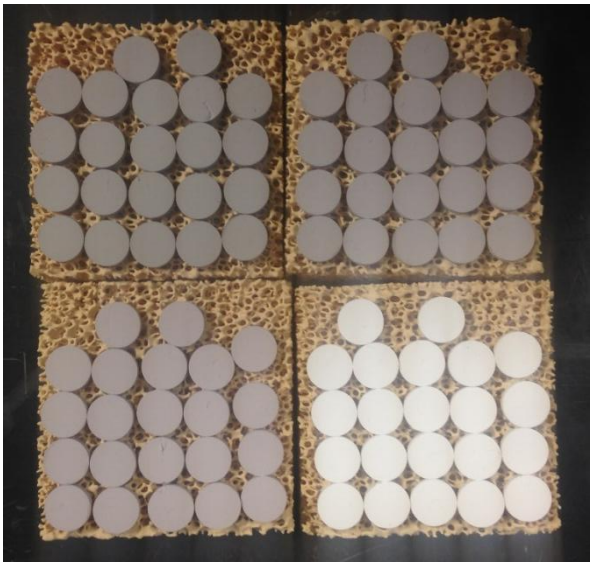

Figure 7. Cu-doped TCP samples on scaffolds for sintering.

2.2.2 Phase Composition, Surface Morphology, and Density

The phase composition of the samples was analyzed with a Rigaku D/MAX diffractometer using CuKα radiation, equipped with an Ni filter at a step size of 0.04° and a count time of 1.5 seconds per step. The relative α-TCP phase intensity compared to the ß-TCP phase intensity was calculated by:

$$\frac{Intensity\ of\ \alpha\ phase}{\Sigma\ Intensity\ of\ \alpha\ and\ ß\ phases} \quad \text{Eq. 1}$$

After applying a thin-layer coating of Pd/Au, microstructure of the top surface of the samples was performed using a field emission scanning electron microscope (FESEM, Hitachi model S4500). Relative bulk and apparent densities were measured by specimen dimension and Archimedes' method. Samples were submerged in boiling water for 2 minutes to ensure all trapped air was removed from internal pores and then immediately submerged in room-temperature water to obtain the wet weight. The relative bulk density of the samples was calculated as mass per volume of each sample divided by the nominal density of TCP, which is 3.07 g/cm^3. The percentage obtained subtracted from 100% gave the total porosity. Apparent density was calculated as the dry weight divided by the difference between dry and wet weight, which, when divided by nominal density, gives relative apparent density. Apparent density subtracted from 100% gives the percentage of closed pores, and by subtracting this percentage from the total porosity percentage, the open porosity can be obtained.

2.2.3 Cell Culture

The human osteoblast cell line hFOB 1.19 (hFOB; see Figure 8) was purchased from ATCC (Manassas, VA) and cultured in complete growth medium (DMEM supplemented with 10% fetal bovine serum (FBS) and antibiotic/antimycotic). Before use, disks were sterilized using an autoclave. Disks were placed in 24 well plates (one disk per well), and hFOB cells were seeded on top of each disk, followed by culturing in the presence of additional cell culture media. All experiments were conducted at 34 ^{o}C in the presence of CO_2.

2.2.4 Assessment of Cell Growth Using XTT Assay

Cells were suspended in complete growth medium at a concentration of 50×10^3 cells/20 µl. TCP disks were placed in triplicate wells of a 24-well plate. Twenty µl of concentrated cells were added to TCP disks and allowed to adhere to the top of each disk, then 400 µl of complete growth media were added to each well. Cells were cultured at 34 ºC in the presence of 5% CO_2 and media was replenished every 3–4 days. After 5 or 10 days, media was carefully removed from the wells and the disks were washed gently with 1 ml of Dulbecco's Phosphate-Buffered Saline (DPBS) (ThermoFisher Scientific, Waltham, MA). TCP disks were then removed and placed into a new 24-well plate, followed by the addition of 400 µl of DPBS and 100 µl of XTT working solution (Trevegin, Gaithersburg, MD), and incubated at 34 ºC for 3 hours, then analyzed on an Epoch plate reader (Biotek, Winooski, VT; see Figure 9).

Figure 8. Osteoblast cells used for cell culture.

Figure 9. Epoch plate reader for XTT.

2.2.5 Assessment of Gene Expression

For gene expression studies, 2×10^6 cells/20 μl were seeded on top of each TCP disk in triplicate wells of 24-well plates, followed by addition of 400 μl cell culture medium. After 1 or 5 days incubation, media was removed and the disks were washed gently with 1 ml DPBS. Samples were placed into new 24-well plates and the cells were immediately lysed using 1 ml TRIzol reagent (ThermoFisher Scientific), and the total RNA was isolated following manufacturer's protocol as previously published [109,118]. Reverse transcription reactions were performed using Moloney murine leukemia virus (M-MLV) reverse transcriptase (Promega, Madison, WI). Quantitative real-time PCR (qPCR) was conducted using the ViiA7 real-time PCR instrument (Life Technologies, Grand Island, NY). Gene expression was calculated by subtracting the threshold cycle (C_T) for the housekeeping gene (GAPDH) from the gene of interest, and relative gene expression was compared to cells grown on pure TCP disks. The following primers were used in this study:

GAPDH, 5'-CTCGACTTCAACAGCGACA- 3' (forward) and
5'-GTAGCCAAATTCGTTGTCATACC-3' (reverse);
OPG, 5'-GTCTTTGGTCTCCTGCTAACTC-3' (forward) and
5'-CCTCACACAGGGTAACATCTATTC-3' (reverse);
COLA1, 5'-CGATGGATTCCAGTTCGAGTATG-3' (forward) and
5'-CTTGCAGTGGTAGGTGATGTT-3' (reverse);
ALP-1, 5'-CCTACCAGCTCATGCATAACA-3' (forward) and
5'-GGCTTTCTCGTCACTCTCATAC-3' (reverse);
OCN, 5'-CAGGCGCTACCTGTATCAAT-3' (forward) and
5'-CGATGTGGTCAGCCAACT-3' (reverse);
VEGF, 5'-GATGAGCTTCCTACAGCACAA-3' (forward) and
5'-CTTTCCCTTTCCTCGAACTGAT-3' (reverse);
IL-6, 5'-TCCAAAGATGTAGCCGCCC-3' (forward) and
5'-CAGTGCCTCTTTGCTGCTTTC-3' (reverse);
TNF-α, 5'-CCAGGGACCTCTCTCTAATCA-3' (forward) and
5'-TCAGCTTGAGGGTTTGCTAC-3' (reverse); and
RANKL, 5'-AGCACATCAGAGCAGAGAAAG-3' (forward) and
5'-TGTCGGTGGCATTAATAGTGAG-3' (reverse).

2.2.6 Statistical Analysis

A one-way analysis of variance (ANOVA) was used to determine the statistical significance between groups. Statistical significance is denoted as * ($p<0.05$), ** ($p<0.01$), *** ($p<0.001$), and **** ($p<0.0001$). Statistical analysis was performed using GraphPad Prism software (La Jolla, CA).

2.3 Results

2.3.1 Phase Analysis

The relative amount of α-TCP for samples sintered at 1150 °C is listed in Table 5. Figure 10 shows XRD patterns of ß-TCP powder after calcination, initial calcination, and after sintering at 1050°C and 1150 °C for pure-TCP, 0.25 Cu-TCP, 0.5 Cu-TCP, and 1.0 Cu-TCP samples. ß-TCP phase was the only phase present in the structure of all samples after calcination and sintering at 1050 °C. An increase in sintering temperature to 1150 °C resulted in the formation of α-TCP in pure-TCP, 0.25 Cu-TCP, and 0.5 Cu-TCP, whereas no secondary phase was observed in 1.0 Cu-TCP.

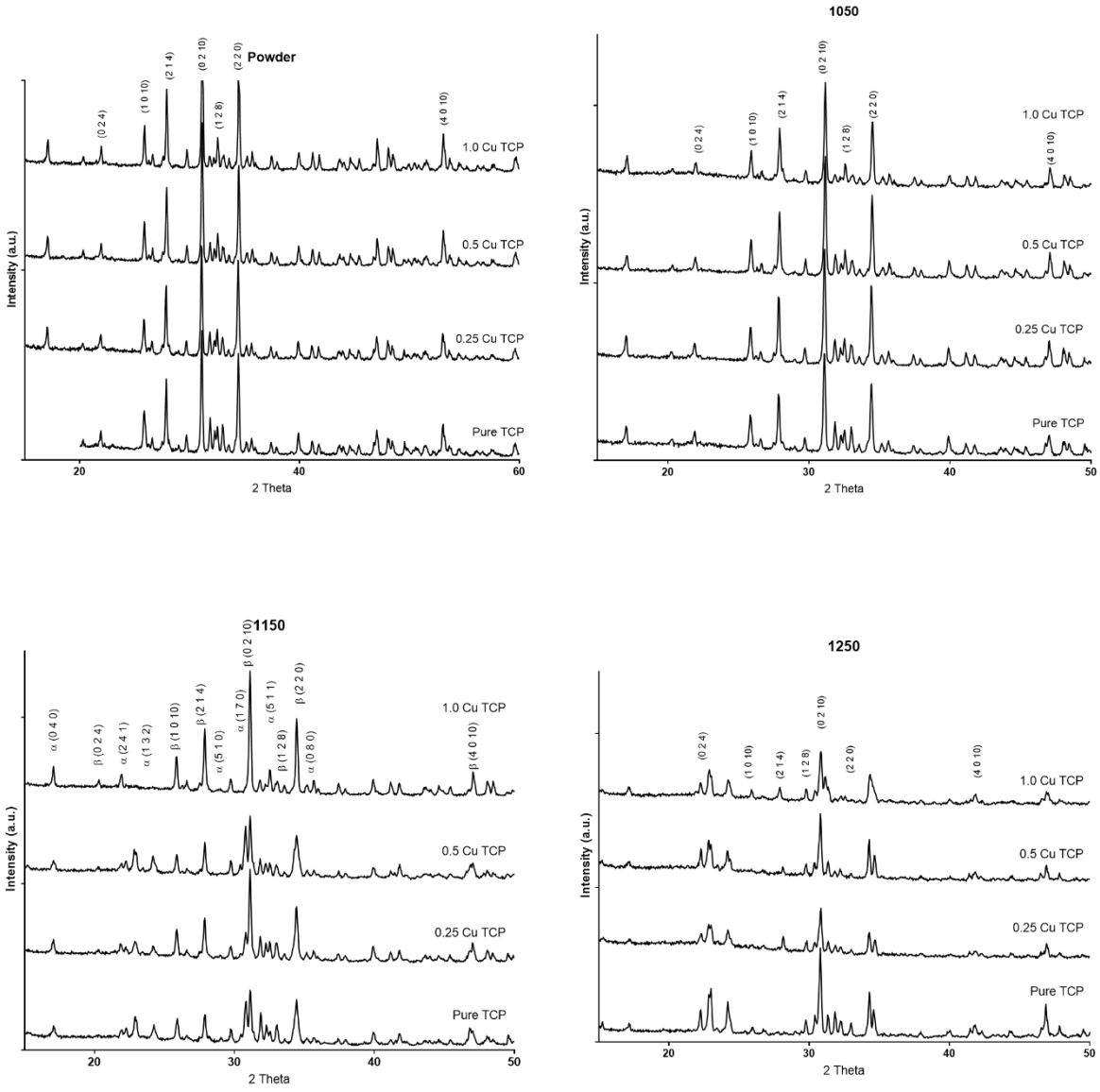

Figure 10. XRD of TCP powder and samples sintered at 1050, 1150, and 1250 °C.

Table 5. α-TCP phase intensity percentages.

	α Intensity (%)
Pure-TCP	17.46
0.25 Cu-TCP	4.92
0.5 Cu-TCP	2.76
1.0 Cu-TCP	0

2.3.2 Density

The total porosity and open porosity of samples sintered at 1050 ºC and 1150 ºC were measured and are shown in Figure 11. In general, the porosity decreased with higher sintering temperature at all concentrations, as shown in Table 6, except at 0.25 Cu-TCP, where the total porosity of 1150 ºC samples was greater than 1050 ºC samples and the open porosity was nearly equivalent. At 1050 ºC, among doped samples, 0.5 Cu-TCP had the greatest total and open porosity with no difference in porosities of 0.25 Cu-TCP and 1.0 Cu-TCP. 0.25 Cu-TCP had the greatest porosity at 1150 ºC, with total porosity decreasing linearly with dopant amount. The open porosity of pure TCP was significantly less at 1150 °C and slightly less at 0.5 Cu-TCP and 1.0 Cu-TCP.

Table 6. Comparison of open and total porosities at different sintering temperatures.

	1050 °C Total Porosity	1150 °C Total Porosity	% Change
Pure TCP	33.74 ±0.51	31.26 ±0.61	7.35
0.25 Cu-TCP	32.45 ±0.14	37.45 ±0.39	-15.41
0.5 Cu-TCP	33.87 ±0.66	33.35 ±0.44	1.54
1.0 Cu-TCP	31.87 ±0.16	31.89 ±0.67	-0.06
	1050 °C Open Porosity	**1150 °C Open Porosity**	**% Change**
Pure TCP	29.6 ±0.95	27.25 ±0.67	7.94
0.25 Cu-TCP	29.84 ±0.03	30.3 ±0.98	-1.54
0.5 Cu-TCP	31.29 ±0.67	28.31 ±0.50	9.52
1.0 Cu-TCP	29.29 ±0.32	28.97 ±0.64	1.09

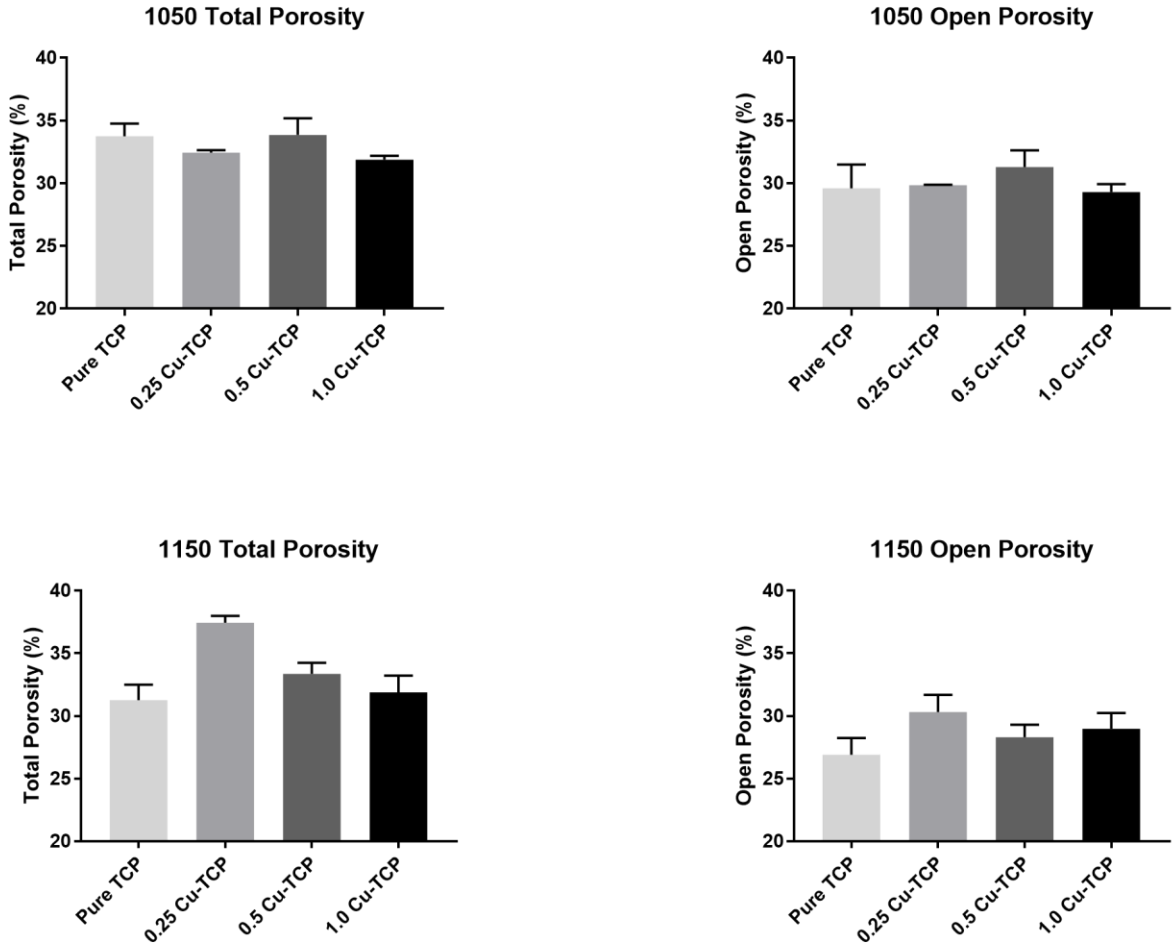

Figure 11. Total and open porosity of TCP samples sintered at 1050 and 1150 °C.

2.3.3 Assessment of Cell Proliferation

XTT assay was used to determine proliferation of osteoblast cells on pure and Cu-TCP samples after 5 and 10 days of culture. OB cells were able to proliferate on pure-TCP samples as evidenced by increased relative proliferation from day 5 to day 10 ($p<0.0001$) and as shown in Figure 12. No difference was found in cell proliferation between pure-TCP and 0.25 Cu-TCP samples at both 5 and 10 days. However, the addition of higher concentrations of Cu resulted in a significant decrease in cell proliferation at both time points in a dose-dependent manner.

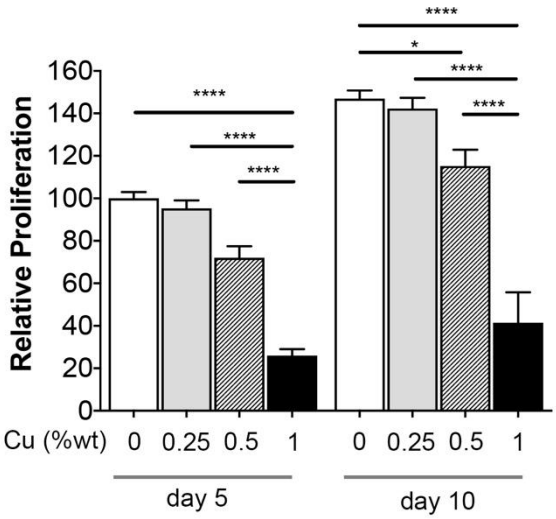

Figure 12. Proliferation of osteoblast cells after 5 and 10 days incubation.

2.3.4 Assessment of Cell Differentiation and Inflammation

In this study inflammatory gene expression by qPCR was evaluated after 1 and 5 days of sample seeding. The addition of Cu to TCP samples did not affect IL-6 expression at day 1 (Figure 13). Furthermore, although IL-6 expression increased in pure TCP samples from day 1 to day 5, IL-6 expression was significantly reduced after 5 days for all Cu-doped samples in a dose-dependent manner. Similar to IL-6, there was significant reduction in TNF-α levels in Cu-doped samples at day 1 and day 5. However, there was an increase in IL-17 expression, particularly in samples doped with a high-percent Cu (1%) at 1 and 5 days.

The expression of several differentiation markers in FOB grown on TCP samples was also examined. It was found that expression of osteoprotegerin (OPG) did not change in the presence of any Cu concentration at an early time point (day 1). However, at day 5, OPG expression was significantly reduced at 1% Cu-TCP compared to pure TCP, despite increased expression of OPG on pure TCP samples at day 5 compared to day 1. The expression of osteocalcin (OCN) was not affected by the presence of Cu on TCP samples at earlier and later kinetics. Similarly, the expression of ALP-1, although initially decreased in the presence of 0.25 and 0.5% Cu on TCP, at 1% Cu, showed no difference, and at later kinetics, ALP-1 expression decreased but was not affected by Cu. This is in contrast to vascular endothelial growth factor (VEGF), collagen type 1 α (COLA-1), and receptor activator of nuclear factor kappa-B ligand (RANKL), where cells grown on 1% Cu-TCP had significantly increased expression at an early time point. However, the presence of Cu did not alter expression at later kinetics.

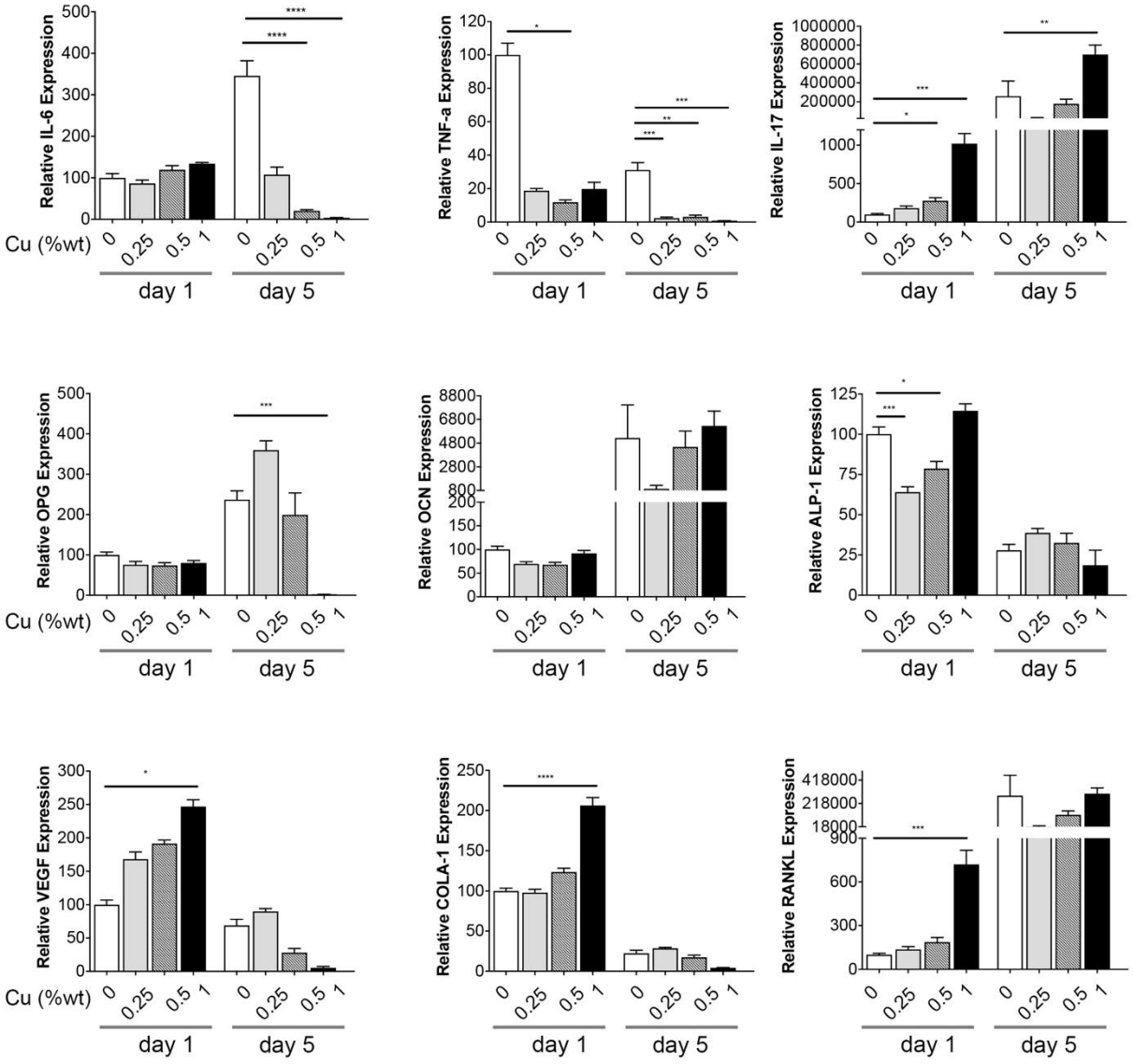

Figure 13. Gene marker expression of osteoblast cells after 1 and 5 days incubation.

2.4 Discussion

Calcium phosphates such as ß-TCP are a viable option for use as bone substitution materials because of their compositional similarity to bone, as well as many other features [68,119]. Though CaPs have limited osteoinductivity, this can be enhanced with the addition of trace elements such as Co, Zn, Si, and Cu. In this study, ß-TCP scaffolds were synthesized via the solid-state method and sintering, and the osteoinductivity and angiogenesis of OB cells, when cultured on pure ß-TCP scaffolds compared to Cu-doped ß-TCP, were examined. The effect of adding Cu to the physical properties of ß-TCP was also studied.

Prior to sintering all samples, two samples at each concentration were sintered at 1050 and 1150 °C. XRD analysis was performed on each sample so that the phases present could be identified. Samples sintered at 1150 °C showed slight occurrences of α-TCP with the greatest intensities of β-TCP phases, whereas the samples sintered at 1050 °C showed only occurrences of β-TCP. Based on these findings, 1150 °C was the chosen sintering temperature for the remainder of the samples. The α-TCP transition generally occurs around 1125 °C [67], which is why there are α-TCP phases present in the 1150 °C samples. The 1050 °C sintering shows no presence of α-TCP, which is expected since the α-TCP transition occurs around 1125 °C.

At high sintering temperatures, trace amounts of Cu were found deposited on the inside of the furnace that was utilized, as shown in Figure 14. This was visibly observed as pink streaks on the heating elements, and pink dots were also noted on the pure TCP samples. The contaminated samples were discarded, and crucibles were utilized to cover all samples to prevent further contamination.

Increased levels of α-TCP result in a decreased dissolution rate compared to β-TCP, which can be seen by the solubility products and calcium-to-phosphate ratios of both calcium phosphates. The solubility product of calcium phosphates increases as the Ca/P ratio decreases. However, the calcium-to-phosphate ratio of both α- and β-TCP is 1.50 [120]. The solubility products of these calcium phosphates, however, differ by a factor of 3, with α-TCP having a higher solubility product than β-TCP [66]. Because of the increasing presence of α-TCP with increasing sintering temperature, it can be concluded that the dissolution rate will increase with increasing sintering temperature and that the stability of the samples therefore decreases with increasing sintering temperature. This same trend was recently observed in lithium-doped TCP and resulted in the decrease of compressive strength at higher sintering temperature [84]. Because of the relatively low α-TCP intensity compared with β-TCP found at 1150 °C, this temperature was chosen as the sintering temperature. The β- to α-TCP transition temperature has been documented as 1125 °C [67], so by sintering at 1150 °C and observing the small amounts of α phase, one can be certain that 1150 °C is a high enough temperature to complete the β-TCP reactions without having excessive occurrence of the α phase.

Figure 14. Cu deposition on furnace heating elements.

The results of this study show that the addition of Cu^{2+} stabilizes the β-TCP crystal structure at 1150 °C, where β-TCP to α-TCP phase transformation is expected [67]. Cu^{2+} incorporation decreases the α-TCP phase in a dose-dependent manner from 17.5 in pure TCP to 4.5, 2.8, and 0 when 0.25, 0.5, and 1.0 wt. % of dopant is added, respectively. Because of the similar valence of Ca^{2+} and Cu^{2+}, the copper ion substitutes the Ca sites in the TCP structure [121]. However, the ionic radius of Cu^{2+} is much smaller than Ca^{2+} (0.73 Å and 0.99 Å, respectively) and replacement of Ca with Cu causes the structural shrinkage, which eventually stabilizes the β-TCP structure. This data is in accordance with previous data that found that Ca^{2+} substitution with smaller Li^{+} and Fe^{3+} reduces the α-TCP occurrence [84,122]. Studying the α-TCP formation is crucial as it increases the solubility product by a factor of 3, so faster dissolution is expected [3].

The decrease in porosity that was observed with higher sintering temperature is expected because at higher temperatures the particles fuse together and there is higher density as a result. This also accounts for the decrease in open porosity for most Cu concentrations at higher temperatures. High temperatures (around 1000–1200 °C) are used to synthesize copper phosphates from CuO, so this may also affect the density [123]. The decrease in open porosity from 1050 to 1150 °C was significant for pure TCP samples but was much less so for the 0.25 and 1.0 Cu-TCP samples, which suggests that Cu addition decreases the effect of increasing sintering temperature on porosity. The same trend is apparent in total porosity as well, with the total porosity decreasing by almost 2.5% for pure TCP but only changing by 0.5 and 0.01% for 0.5 and 1.0 Cu-TCP, respectively. Thus, it is evident that Cu addition contributes to thermal stability in this TCP.

Copper is considered an essential trace element for humans and, because of the role that Cu plays in Cu-binding proteins, Cu deficiencies have been linked to cardiomyopathy, anemia, and many other serious health issues [111,114]. On the contrary, Cu excess has been linked to cirrhosis and decreased liver function, and excess Cu consumption has been shown to cause intestinal cramps and nausea [114]. On a cellular level, Cu toxicity is often credited to the creation of reactive oxygen species (ROS) by Cu ions, which ultimately leads to the breakdown of DNA strands [91]. However, in sufficiently small amounts, Cu has been reported to increase VEGF secretion in a variety of cell types and dopant concentrations [95,116,124]. Likewise, Cu has been observed to increase expression of osteogenic genes such as ALP, OCN, and OPN, though the results of the study by Schamel et al. show similar results between non-doped and doped samples [116,125,126]. In this study, the VEGF expression upregulated at early time points with the presence of Cu in a dose-dependent manner; however, at a later time point, the trend did not continue. This may be due to Cu toxicity and decreased cellular proliferation at 0.5 and 1.0 Cu-TCP, resulting in fewer cells and thus less VEGF expression. Furthermore, the increase at earlier time points may be sufficient to induce a biological effect and sustained levels may no longer be needed. With up to 0.25 Cu-TCP, at both 5 and 10 days, no significant difference in cell proliferation was observed compared to pure TCP. However, at 0.5 Cu-TCP, relative cellular proliferation decreased, and at 1.0 Cu-TCP, significantly less cells were present at both time points compared to pure TCP. This indicates that 0.25 wt. % Cu addition is near the maximum amount of Cu that can be safely utilized as a dopant without negatively affecting cell proliferation.

Varied results were observed for osteoinductive gene expression of ALP and OCN, as there was no difference in the expression of OCN at earlier kinetics between the four samples, but there was an initial decrease in ALP expression in cells grown on 0.25 and 0.5 Cu-TCP and no change at 1.0 Cu-TCP compared to pure TCP. Perhaps the lack of effect on OCN is due to its abundance as a noncollagenous skeletal-derived protein [127]. This study found that ALP expression was initially higher at earlier kinetics and reduced at later kinetics (see Figure 3). This is consistent with the expression of ALP during bone development, where it is highly expressed during early bone development and expression is reduced during later development [128]. Both ALP and OCN are indicators of osteoblast differentiation, and OCN is known to be produced after maturation of the osteoblasts while ALP is an early indicator [50,129]. The observed increase in expression of OCN at the second time point in this study corroborates this data. At early time points, increasing the dopant amount resulted in an increase of COLA-1 expression, but at later kinetics the expression was similar for all concentrations and reduced compared to the Pure-TCP sample at early kinetics. Since ALP is an early indicator of osteoblast differentiation and COLA-1 is expressed prior to ALP, this trend is expected. OPG, as a decoy RANKL receptor, also enhances differentiation, and the absence of OPG has been linked to decreased bone mass in mice [24,130].

This study found that at later kinetics, OPG expression was significantly increased with 0.25 Cu-TCP compared to pure TCP. When RANKL binds with OPG instead of RANK, osteoclastogenesis is prevented, thus leading to enhanced bone formation [24]. IL-6 and TNF-α are both inflammatory genes and both were downregulated with Cu dopant in this study. IL-6 promotes osteoarthritis and also leads to the upregulation of Ank, Anx-5, and Pit-1, which are all genes that lead to calcification [40]. Likewise, increasing TNF-α leads to decreasing ALP expression, decreasing osteoblast differentiation and upregulation of osteoclasts [46,47]. Finally, an increase in IL-17 expression at early and later kinetics was found. IL-17 was found to play a pro-osteogenic role in mesenchymal stem cells (MSCs), therefore the induction of IL-17 expression may play an osteogenic role [44]. Thus, this study found that Cu dopants contribute to the formation of bone and can cause therapeutic inflammation inhibition.

2.5 Conclusion

The effects of Cu addition to TCP scaffolds on phase composition and physical and biological properties were reported in this study. Relative amounts of α-TCP phase intensity were found to significantly decrease with increasing amounts of Cu dopant. In addition, increasing sintering temperature had less of an effect on the open porosity of samples with higher Cu addition. Biologically, Cu dopant increased osteogenic markers and decreased the expression of proinflammatory markers.

CHAPTER 3 COPPER- AND COBALT-DOPED BRC

3.1 Introduction

Dicalcium phosphate dihydrate (DCPD) is one type of CaP that is commonly used because of its relatively high solubility factor of $2.5 \cdot 10^{-7}$, which makes it highly resorbable. As a cement, it has high injectability and moldability, and DCPD has increased osteoinductivity compared to other CaPs, which leads to improved bone remodeling [66,131]. The osteoinductivity of DCPD is, however, still relatively low, so many methods have been used to enhance this property, including the incorporation of growth factors and ionic substitution [76,132]. This study evaluated the effects of doping brushite cement (BrC), a precipitate of DCPD, with Cu and Co.

Copper (Cu) is an essential trace element in the body, helping the body to handle oxidative stress and defend against antioxidants [133]. As mentioned previously, the osteoinductive properties of BrC are limited, and methods have been explored to enhance these properties. Gene markers such as VEGF, ALP, OCN, OPG, and others are good indicators of bone growth, and the maximization of their expression is desired. Growth factors can enhance these markers, as can metal dopants, which were utilized in the present study. Co has been found to increase VEGF expression when added to hydroxyapatite scaffolds, and Fe increased ALP expression when added to ß-TCP [122,134]. The physical properties of calcium phosphates are also altered by the addition of metal ions; the study by Vahabzadeh et al. showed an increase in compressive strength and density with the addition of trace amounts of Li [84]. Another study by Bose et al. showed a significant decrease in compressive strength with the addition of Mg, Sr, and Si, and showed the effects on grain size with the addition of these dopants [110]. Cu as a dopant in various calcium phosphate biomaterials has been well documented as integral in blood vessel formation, and angiogenesis-related gene expression, such as VEGF, has been shown to increase with Cu stimulation [94,135–137]. Wu et al. showed that copper-doped mesoporous bioactive glass stimulated alkaline phosphatase (ALP), osteopontin (OPN), and osteocalcin (OCN) expression in human bone marrow stromal cells in a dose-dependent manner [116]. In another study, ALP activity of MC3T3-E1 mouse preosteoblast cells also increased up to 0.8 wt. % Cu addition in silicate bioactive glass [138]. However, Li et al. directly treated human umbilical vein endothelial cells (HUVEC) with $CuSO_4$ and found that the expression of VEGF was not affected by Cu stimulation [139]. Li et al. also demonstrated Cu cytotoxicity at levels above 200 μmol/L [139]. Another study showed an increase in human mesenchymal stem cell proliferation up to 0.1 mM Cu addition to Ti-64 plates, and no cytotoxicity up to 0.5 mM Cu addition [140].

Recently, cobalt (Co) has been considered for use in different CaP systems [134,141,142]. Co is present in bone, dentine, and enamel with maximum concentration of 1 ppm [65] and is part of vitamin B12. Vitamin B12 (also known as cobalamin) plays an important role in DNA synthesis and neurological function, and its deficiency is associated with hematologic disorders as well as neuropsychiatric disorders [143]. Reported findings show the effective role of Co^{2+} in stabilizing the hypoxia inducible factor-1α (HIF-1α) and in inducing the angiogenesis [144]. Although hypoxia (low oxygen levels, 3% O_2) is important in development and wound healing, dysregulated hypoxia plays an important role in several diseases such as cancer, and heart and lung disease [145]. In fact, tumor hypoxia is one of the most common conditions encountered in the tumor microenvironment and activates HIF-1α, which leads to the activation of a

transcriptional program that allows cells to adapt to this hypoxic environment and drives tumorigenesis [145]. Furthermore, a role for hypoxia in promoting inflammatory gene expression has been described, where it induces expression of interleukin 6 (IL-6), a cytokine that promotes tumorigenesis [145–147]. Among the different osteosarcoma cell lines, MG-63 is a suitable candidate to study the effects of different compositions and biomolecules on proliferation and differentiation of malignant bone cells, *in vitro* [148,149]. Therefore, this study examined the effects of Co concentration on short-term proliferation and expression of HIF-1α in the MG-63 cell line under normoxic and hypoxic conditions.

This study hypothesized that the addition of Cu and Co, in various concentrations, to BrC will alter the microstructure, phase composition, compressive strength, setting time, osteoblast and MG-63 osteosarcoma cell growth (under normoxic and hypoxic conditions), and gene expression. To validate this hypothesis, appropriate amounts of Cu and Co were added to TCP precursors, and DCPD cement samples were produced. These samples were evaluated by x-ray diffraction (XRD) and scanning electron microscopy (SEM) to characterize the phase composition and microstructure. Setting time was determined using a Gillmore needle, and compressive strength was evaluated. To determine the biological impact of Cu addition, quantitative real-time polymerase chain reaction (qPCR) and XTT (2,3-bis-(2-methoxy-4-nitro-5-sulfophenyl)-2H-tetrazolium-5-carboxanilide) techniques were utilized.

3.2 Materials and Methods

3.2.1 Powder Preparation

To process the TCP powder, solid-state synthesis was used as explained in reference [106]. In brief, two moles of calcium hydrogen phosphate ($CaHPO_4$, Alfa Aesar, >98.0%) and one mole of calcium carbonate ($CaCO_3$, Alfa Aesar, >99.0%) were ball-milled for 2 hours at a powder: milling media ratio of 1:4. The mixture was then calcined for 24 hours at 1050 °C in a muffle furnace and cooled naturally to room temperature. The 0.25, 0.5, and 1.0 wt. % copper- or cobalt-doped tricalcium phosphate was prepared by adding proper amounts of copper oxide or cobalt oxide to the TCP precursors and then processed identically to undoped TCP (Figure 15). The (Ca+Cu or Co)/P molar ratio was kept at 1.5 during the entire process for the different concentrations of Cu and Co.

Following calcination, half of the TCP was kept as coarse powder, and the other half was made into fine powder through mixing with ethanol and milling media for 6 hours at a powder: ethanol: milling media ratio of 1:1.5:5 and then drying at 65 °C for 3–4 days.

Figure 15. Doped TCP powders in crucibles after calcination.

3.2.2 Cement Preparation

To prepare cement powder, fine TCP, coarse TCP, and calcium phosphate monobasic monohydrate (MCPM, $Ca(H_2PO_4)_2 \cdot H_2O$, Sigma-Aldrich) were mixed by mortar and pestle at a ratio explained in reference [76]. Three grams of this powder were mixed consistently with 900 µl of a polyethylene glycol (PEG, 2 wt. % in nanopure water) solution for 30 seconds and poured into a 7-mm-diameter mold. The mold was covered and incubated at 37 °C and 100% humidity for 1 hour. Samples were removed from the mold and kept in a phosphate-buffered saline (PBS) solution for 24 hours to complete the setting reaction.

3.2.3 Phase Composition and Surface Morphology

The phase composition of the samples was analyzed by x-ray diffraction with a Rigaku D/MAX diffractometer using CuKα radiation, a step size of 0.04º, a count of 1.5 seconds per step, and an Ni filter. Calcined ß-TCP and BrC powders were analyzed, and the relative DCPD phase intensity compared to ß-TCP phase intensity was calculated for the brushite cement by:

$$\frac{Intensity\ of\ DCPD\ phase}{\Sigma\ Intensity\ of\ DCPD\ and\ ß\ phases} \qquad \text{Eq. 2}$$

The surface microstructure of the samples was captured by a field emission scanning electron microscope (FESEM, Hitachi model S4500) after a thin layer of Pd/Au was applied to the top surface.

3.2.4 Setting Time

Gillmore needles were used to measure the initial and final setting times. The cement was prepared as described above and then poured into the mold. The 0.83-in.-diameter 0.25-lb. needle was used to determine the initial setting time, and the 0.042-in.-diameter 1-lb. needle was used to determine the final setting time. Time was recorded from the moment when the cement was poured into the mold until the time when the corresponding needle ceased to indent the surface of the cement.

3.2.5 Compressive Strength

Compressive strength was measured with a 10-kN load cell. The sample was mounted in the center of the fixture and compressed until failure was sustained. The maximum force applied was recorded, and the compressive strength was calculated from this value and the area of the samples.

3.2.6 Cell Culture

The human osteoblast cell line hFOB 1.19 (hFOB) was purchased from ATCC (Manassas, VA) and maintained in complete growth medium (DMEM) supplemented with 10% fetal bovine serum (FBS) and antibiotic/antimycotic. The MG-63 osteosarcoma cell line was purchased from ATCC and maintained in Eagle's minimum essential medium (EMEM) supplemented with 10% heat-inactivated FBS and antibiotic/antimycotic. Disk samples were sterilized with 100% ethanol for 6 hours and dried under sterilized conditions (Figure 16) prior to use. Disks were then placed in 48-well plates (one disk per well) and seeded with hFOB cells for the Cu study and MG-63 cells for the Co study on top of each disk, followed by the addition of cell culture media. All experiments were conducted in the presence of CO_2 at 34 ºC for the hFOB and 37 °C for the MG-63.

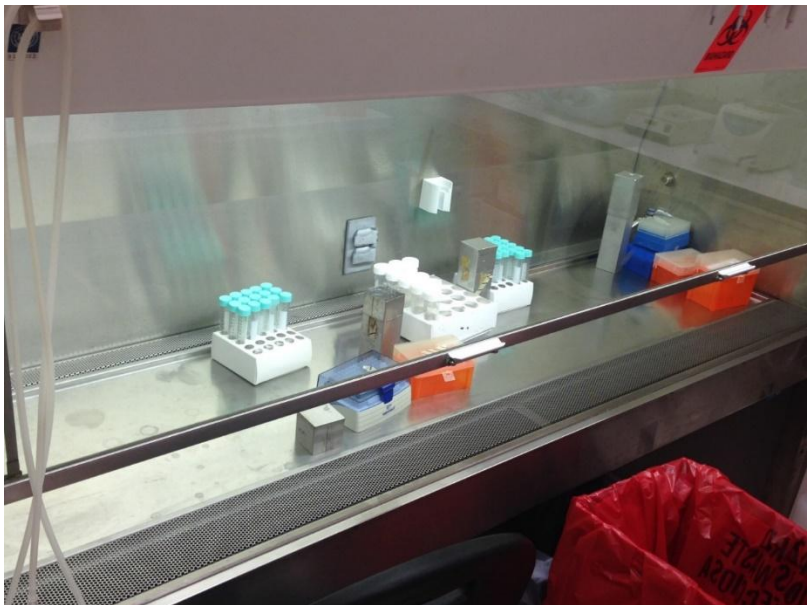

Figure 16. Sterile cell culture hood located in department of biology.

3.2.7 Assessment of Cell Growth Using XTT Assay

Cells were suspended in complete growth medium at a concentration of 25×10^3 cells/20 µl. BrC disks were placed in triplicate wells of a 48-well plate. Twenty µl of concentrated cells were added to BrC disks and allowed to adhere to the top of each disk, then 400 µl of complete growth media were added to each well. Cells were cultured at 34 ºC in the presence of 5% CO2, and media was replenished every 3–4 days for the Cu study. For the Co study, cells were incubated under normoxic (21% O2) or hypoxic (1% O2) conditions. After 1, 3, 5, or 7 days, media was carefully removed from the wells and the disks were washed gently with 1 ml DPBS (ThermoFisher Scientific, Waltham, MA). BrC disks were then removed and placed into a new 48-well plate followed by the addition of 400 µl of DPBS and 100 µl of XTT working solution (Trevegin, Gaithersburg, MD) and incubated at 37 ºC for 3 hours, and then analyzed on an Epoch plate reader (Biotek, Winooski, VT).

3.2.8 Assessment of Gene Expression

For gene expression studies, 2×10^6 cells/20 µl were seeded on top of each BrC disk in triplicate wells of 48-well plates, followed by the addition of 400 µl of cell culture medium (Figure 17). For the Co study, the cells were then incubated under normoxic (21% O2) or hypoxic (1% O2) conditions, whereas all conditions were normoxic for the Cu study. After 1-, 3-, 5-, or 7-day incubation, media was removed and the disks were washed gently with 1 ml DPBS. Samples were placed into new 48-well plates and the cells were immediately lysed using 1 ml TRIzol reagent (ThermoFisher Scientific), and the total RNA was isolated following manufacturer's protocol as previously published [109,118]. Reverse transcription reactions were performed using Moloney murine leukemia virus (M-MLV) reverse transcriptase (Promega, Madison, WI). Quantitative real-time PCR (qPCR) was conducted using the ViiA7 real-time PCR instrument

(Life Technologies, Grand Island, NY). Gene expression was calculated by subtracting the threshold cycle (C_T) for the housekeeping gene (GAPDH) from the gene of interest, and the relative gene expression was compared to cells grown on pure BrC disks. The following primers were used in this study:

GAPDH, 5'-CTCGACTTCAACAGCGACA- 3' (forward) and
5'-GTAGCCAAATTCGTTGTCATACC-3' (reverse);
OPG, 5'-GTCTTTGGTCTCCTGCTAACTC-3' (forward) and
5'-CCTCACACAGGGTAACATCTATTC-3' (reverse);
COLA1, 5'-CGATGGATTCCAGTTCGAGTATG-3' (forward) and
5'-CTTGCAGTGGTAGGTGATGTT-3' (reverse);
ALP-1, 5'-CCTACCAGCTCATGCATAACA-3' (forward) and
5'-GGCTTTCTCGTCACTCTCATAC-3' (reverse);
OCN, 5'-CAGGCGCTACCTGTATCAAT-3' (forward) and
5'-CGATGTGGTCAGCCAACT-3' (reverse);
VEGF, 5'-GATGAGCTTCCTACAGCACAA-3' (forward) and
5'-CTTTCCCTTTCCTCGAACTGAT-3' (reverse);
IL-6, 5'-TCCAAAGATGTAGCCGCCC-3' (forward) and
5'-CAGTGCCTCTTTGCTGCTTTC-3' (reverse);
TNF-α, 5'-CCAGGGACCTCTCTCTAATCA-3' (forward) and
5'-TCAGCTTGAGGGTTTGCTAC-3' (reverse); and
RANKL, 5'-AGCACATCAGAGCAGAGAAAG-3' (forward) and
5'-TGTCGGTGGCATTAATAGTGAG-3' (reverse).

For expression of HIF-1α and glioma-associated oncogene family zinc finger 2 (GLI2) relative to the expression of the housekeeping gene, GAPDH, the following primers were used:

b-actin, 5¢-CTCGACTTCAACAGCGACA-3¢ (forward) and
5-GTAGCCAAATTCGTTG TCATACC-3¢ (reverse);
GLI2, 5¢-CTCCGAGAAGCAAGAAGCCA-3¢ (forward) and
5-GATGCTGCGGCACTCCTT-3¢ (reverse);
HIF-1α, 5 ¢-AACATAAAGT CTGCAACATGGAAG-3¢ (forward) and
5¢-TTTGATGGGTGAGGAATGGG-3¢ (reverse).

3.2.9 Statistical Analysis

A one-way analysis of variance (ANOVA) was used to determine statistical significance between groups. Statistical significance is denoted as * ($p<0.05$), ** ($p<0.01$), *** ($p<0.001$), and **** ($p<0.0001$). Statistical analysis was performed by GraphPad Prism software (La Jolla, CA).

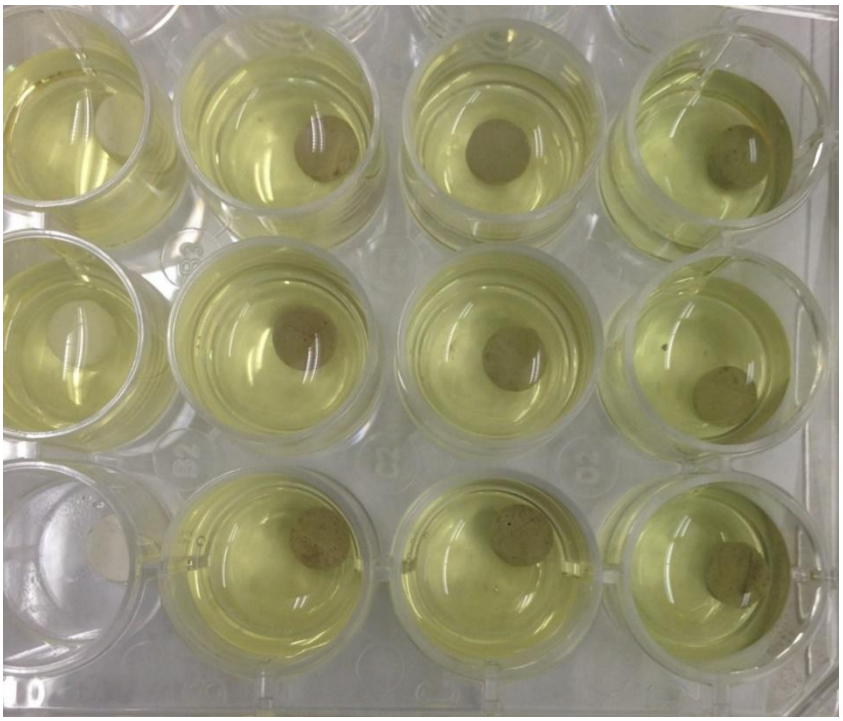

Figure 17. Brushite cement samples for qPCR.

3.3 Results

3.3.1 Phase Analysis

3.3.1.1 Cu-BrC Phase Analysis

The XRD data shows peaks from ß-TCP and DCPD, indicating formation of both phases as expected. Table 7 lists the measured intensity of the 100% peaks of DCPD and ß-TCP (JCPDS 09-0077, 100% intensity at 21º, and JCPDS 09-0169, 100% intensity at 31.1º, respectively). The intensity of the DCPD phase significantly decreased with all Cu addition, with a less notable fluctuation in ß-TCP intensity as shown in Figure 18 and Figure 19. Comparing ß-TCP phase intensity to DCPD, there is a bell curve in the doped Cu data of DCPD that is inverted for ß-TCP. The relative DCPD phase intensity (calculated by Eq. 2) also decreased with Cu dopant.

Table 7. Copper DCPD and ß-TCP phase intensity.

	Pure-BrC	0.25 Cu-BrC	0.5 Cu-BrC	1.0 Cu-BrC
DCPD Phase Intensity (a.u.)	1459	455	721	414
ß-TCP Phase Intensity (a.u.)	1605	2043	1317	2119
Relative % DCPD	47.6	18.2	35.4	16.3

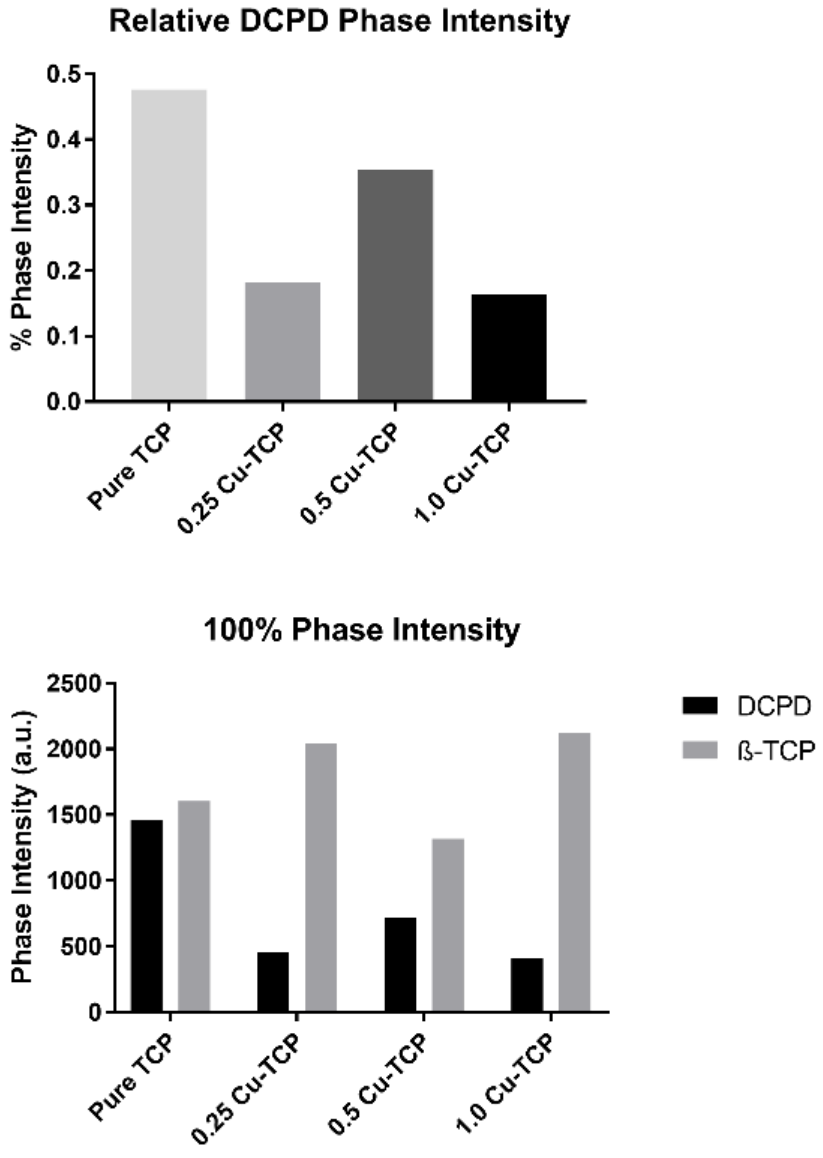

Figure 18. Copper DCPD and ß-TCP phase intensity.

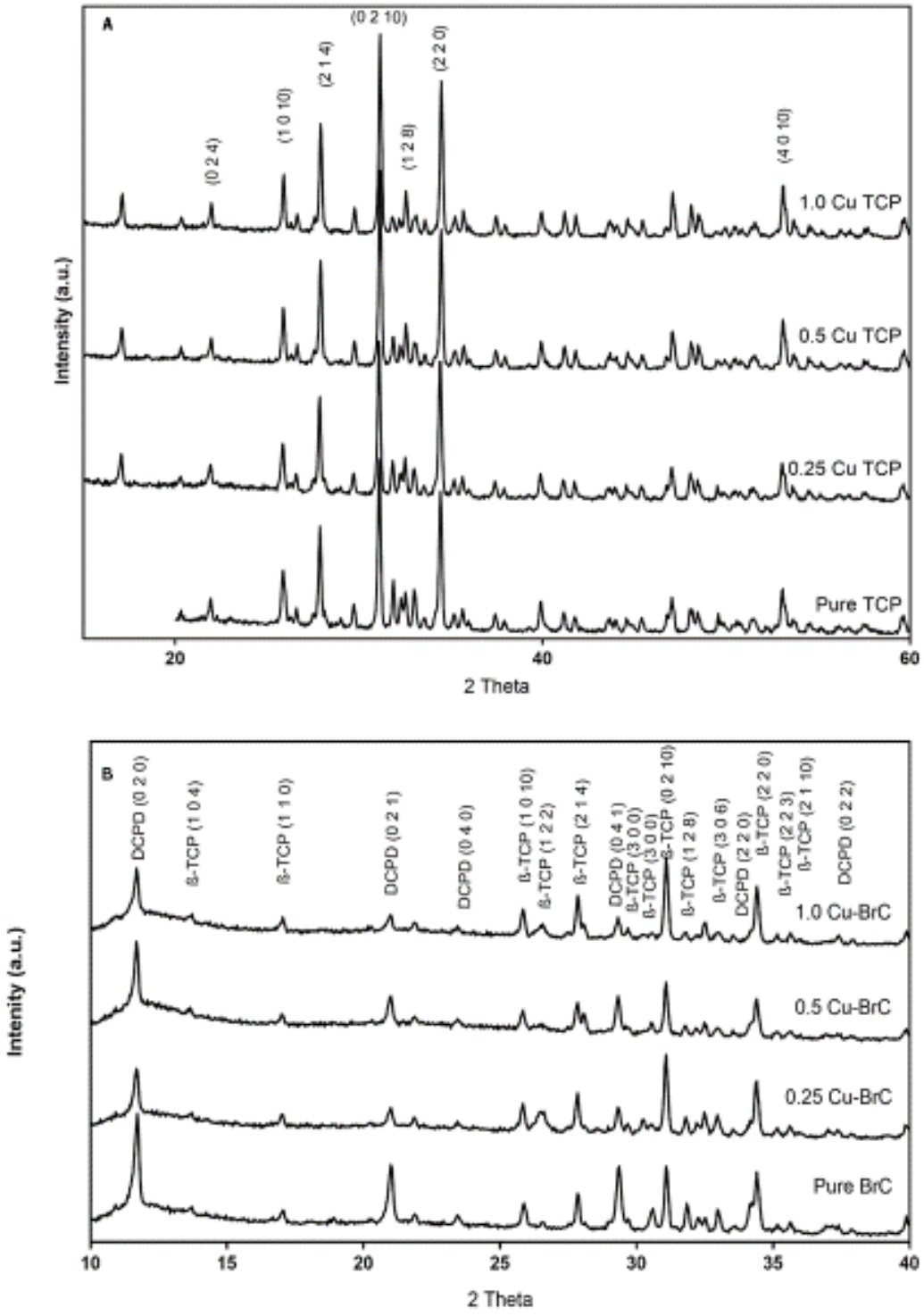

Figure 19. Copper TCP and BrC XRD graphs.

3.3.1.2 Co-BrC Phase Analysis

Processed TCP in the current study was used as the precursor to fabricate the BrCs. As a result, phase analysis of TCP powders containing different concentrations of Co was necessary. XRD spectra of different TCP powders, calcined at 1050 °C, is presented in Figure 20. The results show that the ß-TCP (JCPDS No. 09-0169) was the only phase in pure and doped samples. No other phase including Co was found in the TCP samples.

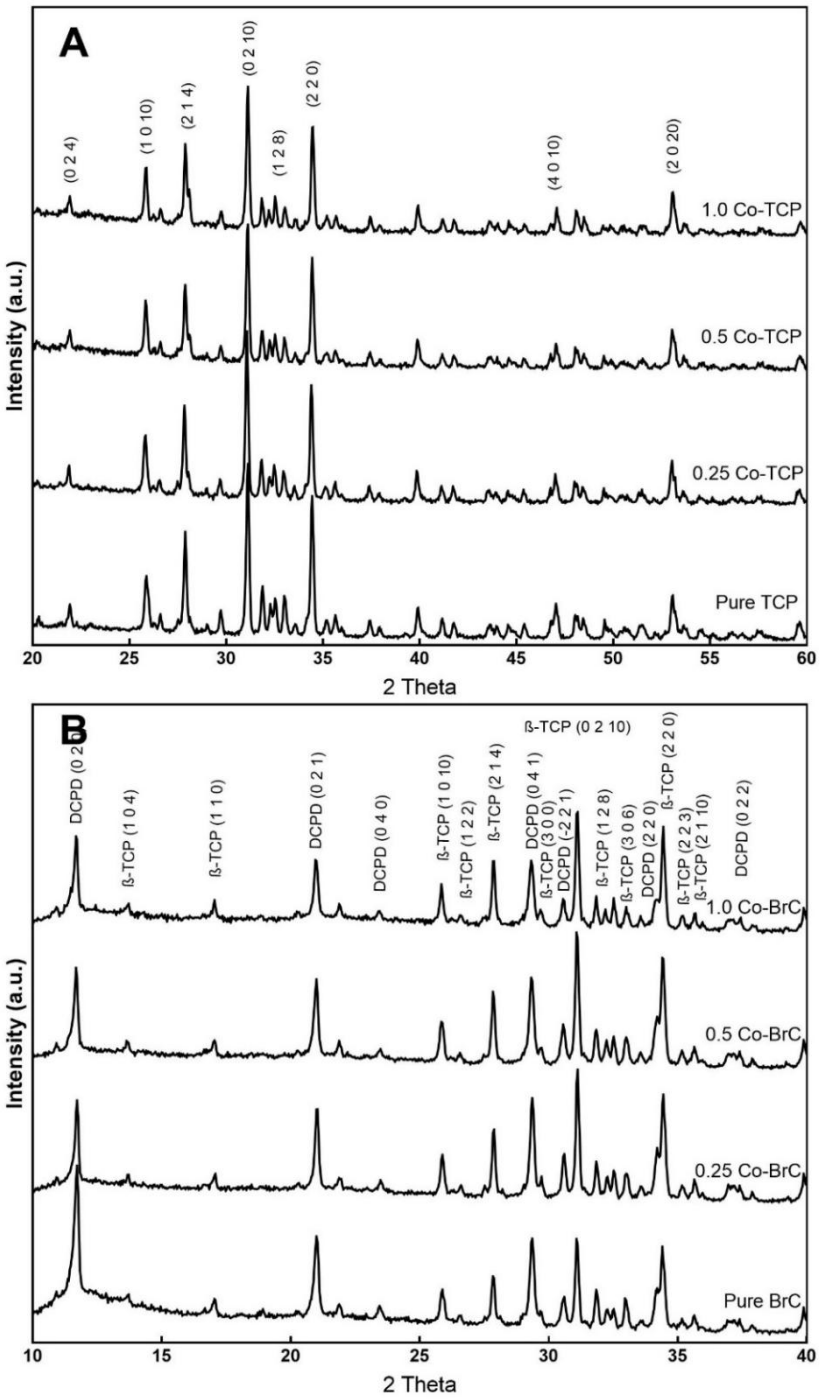

Figure 20. Cobalt TCP and BrC XRD graphs.

3.3.2 Surface Morphology

SEM microstructure of pure and Co-BrC samples shows the presence of granular TCP along with needle/plate-like DCPD throughout the fracture surface of the specimen in Figure 21 [106]. This data is in line with the results from XRD that showed the presence of both phases in all samples.

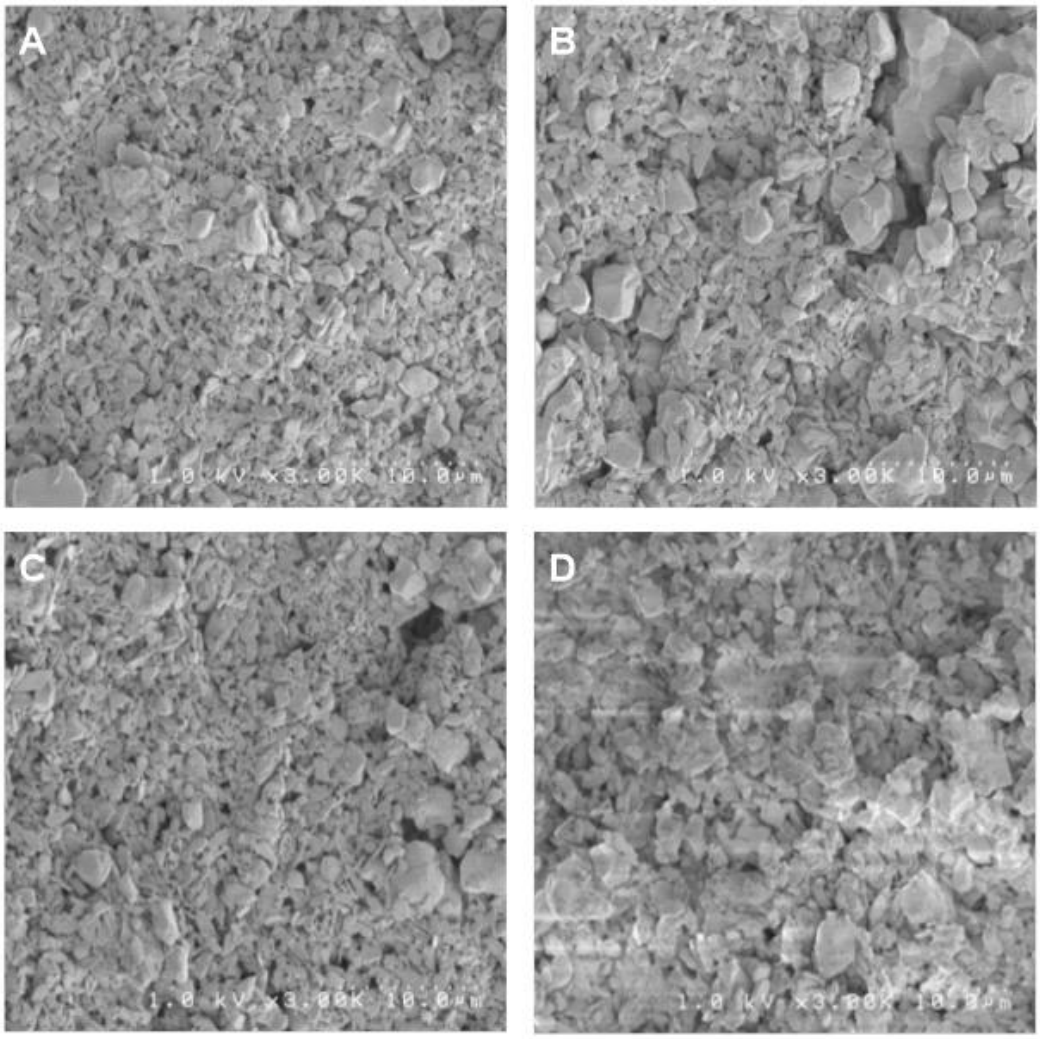

Figure 21. Cobalt BrC SEM images.

3.3.3 Setting Time

3.3.3.1 Cu-BrC Setting Time

Figure 22 shows that increasing Cu content causes an increase in both initial and final setting times. The most significant increase in setting time was observed between 0.5 and 1.0 Cu-BrC. The initial setting time of 0.5 Cu-BrC was just over 7.5 minutes, whereas the initial setting time of 1.0 Cu-BrC was nearly double that. This is especially significant compared to the difference between 0.25 and 0.5 Cu-BrC, which was only about 1 minute, though the initial setting time of pure Cu-BrC was nearly half that of 0.25 Cu-BrC. This same general trend was observed in final setting times as well, with a final setting time of 1.0 Cu-BrC nearly 3 times that of 0.5 Cu-BrC. The difference between pure Cu-BrC and 0.25 Cu-BrC was slightly less compared to the initial setting time, however.

3.3.3.2 Co-BrC Setting Time

The setting time of BrC doped with Co (see Figure 23) increased with increasing amounts of Co, but a slight decrease in setting time was observed between pure BrC and 0.25 Co-BrC. The setting time of 0.5 Co-BrC and pure BrC was nearly the same for both initial and final setting times. A significant decrease in setting time was observed between 0.5 and 1.0 Co-BrC for both initial and final setting times.

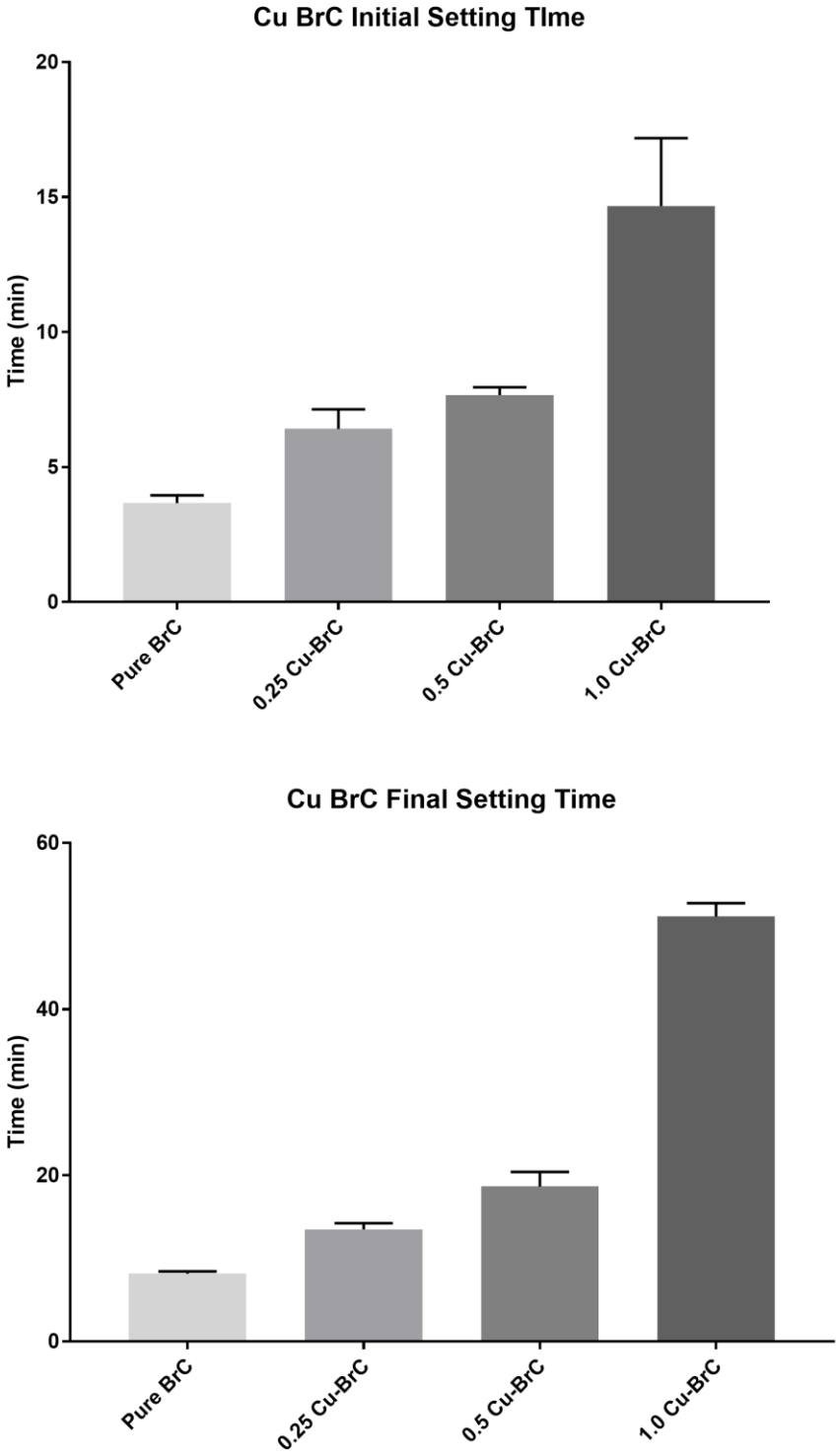

Figure 22. Copper BrC initial and final setting times.

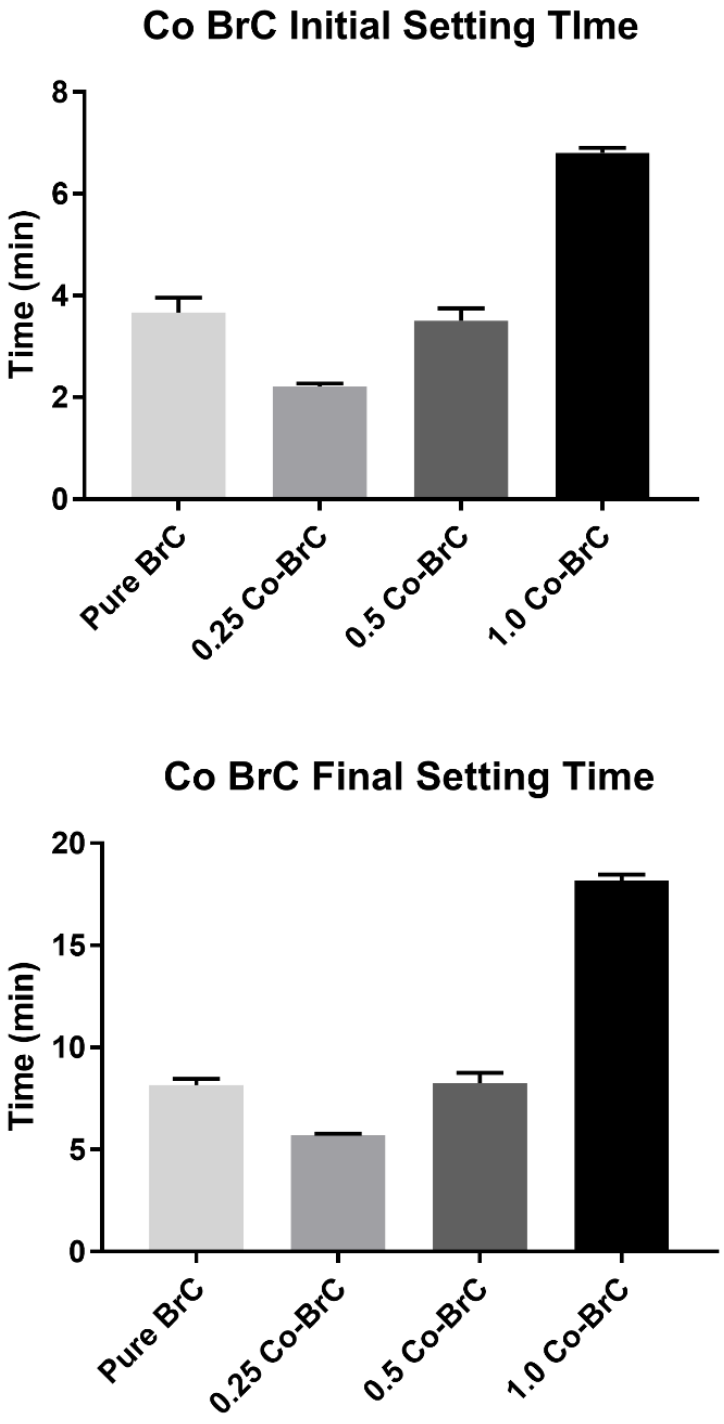

Figure 23. Cobalt BrC initial and final setting times.

3.3.4 Compressive Strength

A clear bell curve is shown in Figure 24 from the results of compressive strength testing. The highest values of compressive strength occurred with 0.25 Cu-BrC, at which compressive strength of 6.3 MPa was recorded, while values for pure Cu-BrC and 0.5 Cu-BrC were nearly identical at 2.9 MPa and 3.3 MPa, respectively. The addition of 1.0 Cu-BrC significantly decreased compressive strength to 0.5 MPa.

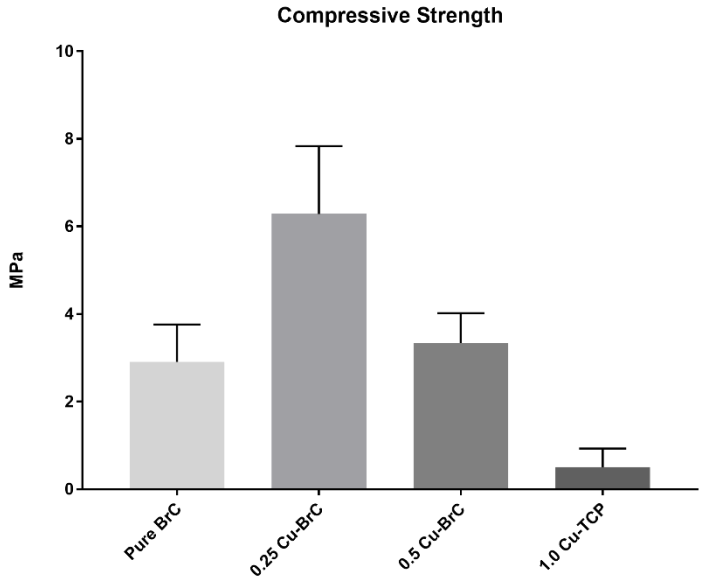

Figure 24. Copper BrC compressive strength.

3.3.5 XTT Assay

XTT assay was conducted to determine cell proliferation when cultured in the presence of pure, Cu-doped, and Co-doped BrC samples. The relative increase in osteoblast proliferation on pure BrC samples from day 3 to day 7 in Figure 25a suggests that OB cells were able to proliferate. The addition of Cu at all concentrations did decrease proliferation in a dose-dependent manner, though cells were able to proliferate as evidenced by the increase in relative proliferation between day 3 and day 7 for all Cu concentrations. Results in Figure 25b show that although there was a modest (20%) increase in MG-63 cell growth on pure BrC under hypoxia compared with normoxia, this increase did not reach statistical significance (Figure 25a). Furthermore, the presence of Co at different concentrations did not affect MG-63 cell growth on BrC under normoxic or hypoxic conditions.

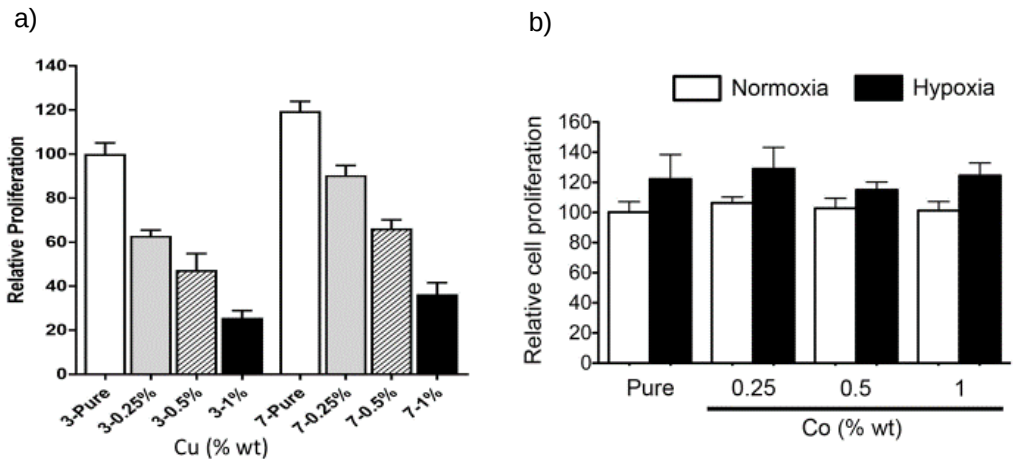

Figure 25. Relative osteoblast and MG-63 osteosarcoma cell proliferation.

3.3.6 Gene Expression

3.3.6.1 Cu-BrC Gene Expression

Gene expression by the osteoblast cells was determined by the qPCR technique, and results are shown in Figure 26. Cells were harvested after 1-, 3-, and 7-day time points, and interleukin 6 (IL-6), tumor necrosis factor α (TNF-α), interleukin 17 (IL-17), osteoprotegerin (OPG), receptor activator of nuclear factor kappa-B ligand (RANKL), alkaline phosphatase 1 (ALP-1), vascular endothelial growth factor (VEGF), collagen type 1 alpha (COLA-1), and osteocalcin (OCN) gene expressions were evaluated. At early time points, IL-6, TNF-α, OPG, ALP-1, and VEGF expression increased with increasing Cu content, but at later time points the trend was reversed. RANKL and IL-17 expression did not occur until day 3, after which point increasing Cu amount corresponded to increasing gene expression. OCN expression showed consistent increase with increasing Cu for all three time points, as did COLA-1, until day 7 when all samples showed limited expression.

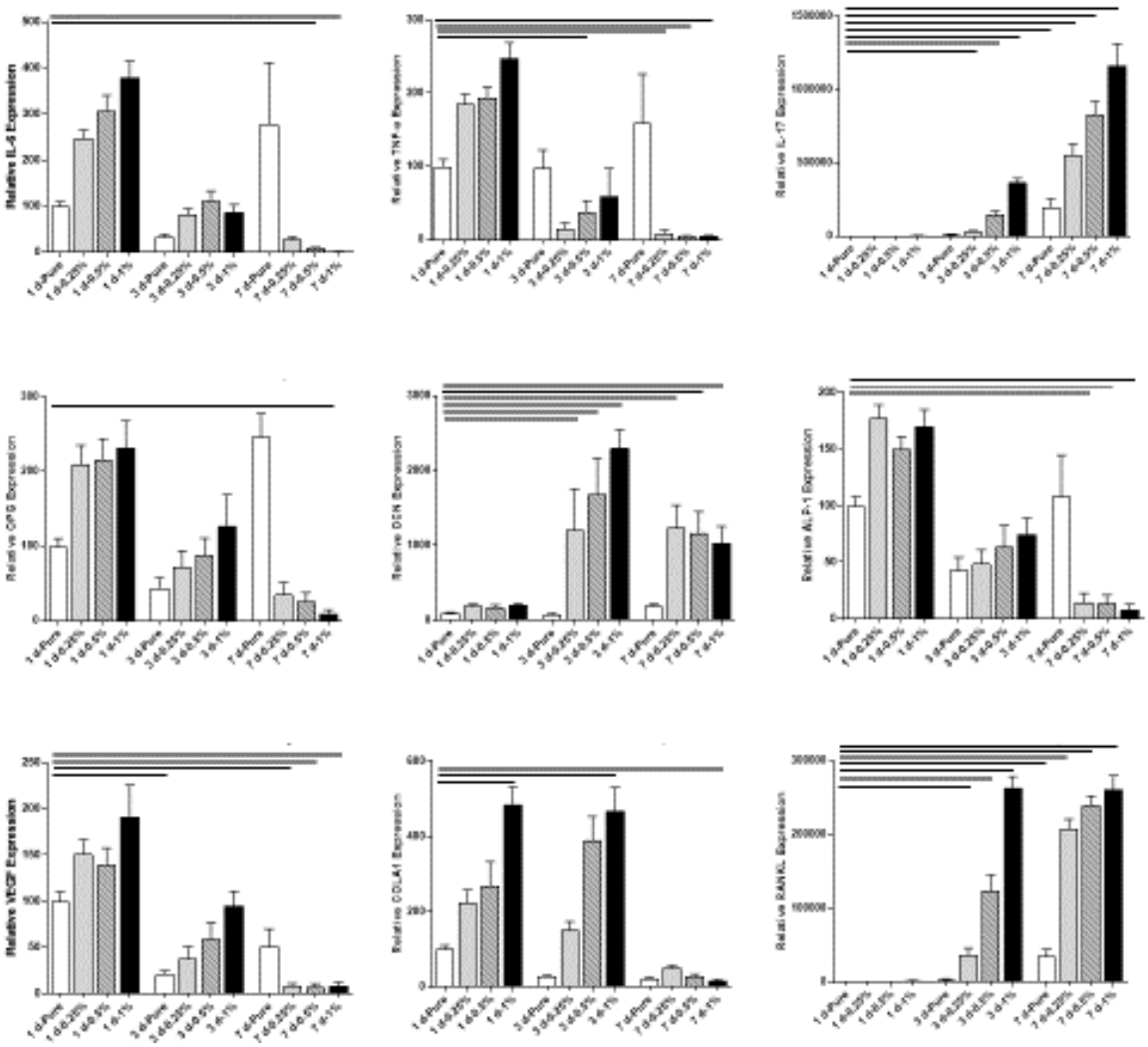

Figure 26. Gene marker expression of osteoblast cells after 1, 3, and 7 days of incubation.

3.3.6.2 Co-BrC Gene Expression

Hypoxia is known to induce the expression of HIF-1α, so the expression of HIF-1α in this study was conducted under normoxic and hypoxic conditions on scaffolds with varying concentrations of Co dopant. The expression of HIF-1α was significantly upregulated in hypoxic conditions on pure-BrC scaffolds compared to normoxic conditions, as was GLI2 expression (Figure 27a,b). Co dopant did not affect HIF-1α expression under normoxic conditions, though its expression was reduced in cells cultured on 0.25 Co-BrC scaffolds (Figure 27c). Similarly, no difference in GLI2 expression was observed with Co addition under normoxic conditions, though 1.0 Co-BrC scaffolds caused a decrease in GLI2 expression under hypoxia (Figure 27d).

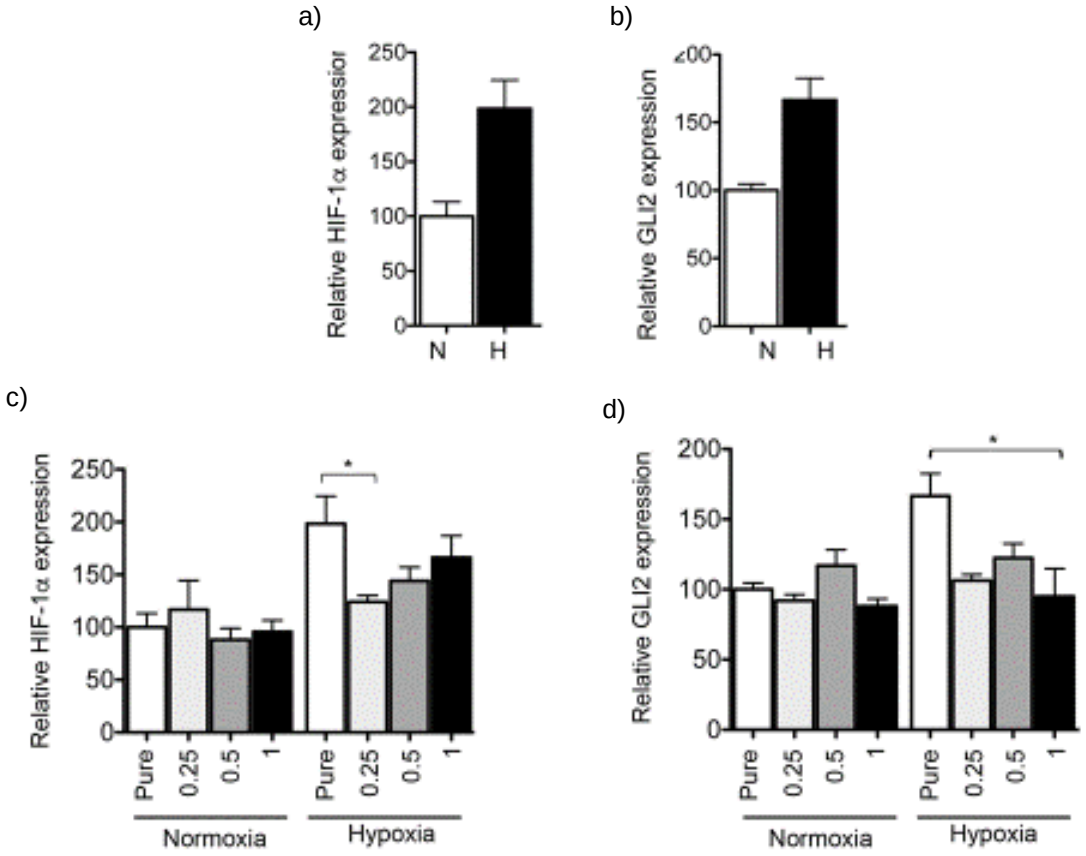

Figure 27. HIF-1α and GLI2 expression under hypoxia and normoxia.

3.4 Discussion

Because of its compositional similarity to bone and its properties such as injectability, brushite cement is a feasible option for use in bone substitute applications. The limited osteoinductivity of most CaPs such as BrC can be enhanced with the use of growth factors or, as shown in this study, through the use of ionic substitutions. Specifically, this study examined the biological and physical effects of doping BrC scaffolds with Cu and Co. This was accomplished by synthesizing TCP powder via the solid-state method, and then mixing it with MCPM, PEG, and water to make the cement. Samples were seeded with OB or MG-63 osteosarcoma cells that were allowed to grow on pure and doped samples to quantify the difference in growth and gene expression with the addition of Cu or Co. The microstructure of the samples was analyzed using XRD and SEM, and the setting time and compression strength were also measured.

The precipitation of BrC occurs by mixing coarse and fine TCP powder with MCPM through the following chemical reaction [150]:

$$\mathbf{Ca_3(PO_4)_2 + Ca(H_2PO_4)_2 \times H_2O + 7H_2O \rightarrow 4(CaHPO_4 \times 2H_2O)}$$

The endothermic dissolution of MCPM, followed by the exothermic dissolution of ß-TCP, begins the precipitation reaction, which ends with an exothermic precipitation of BrC and an increase in the system pH. All samples were prepared in the same manner, with the amount of Cu or Co dopant being the only variable.

3.4.1 Cu-BrC Discussion

The ionic radius of Cu^{2+} is 73 pm, while the ionic radius of Ca^{2+} is 99 pm. The Cu ion is known to substitute for the Ca ion, which decreases the lattice size and increases stability. This increase in stability results in a decrease of dissolution rate and an increase in setting time. The phases of both the TCP powder and the brushite cement were characterized to highlight the phase change between the two. As anticipated, ß-TCP (JCPDS 09-0169) phases were present and dominant in the TCP powder. The transition between ß-TCP to α-TCP generally occurs around 1125 °C, so the calcination of TCP at 1050 °C did not induce the α phase [67]. The impact of Cu addition on the physical properties is clearly shown in the XRD data of the BrC. Within the doped samples, as the phase intensity of the DCPD increases, the phase intensity of ß-TCP decreases and a distinct bell curve in DCPD intensity can be seen from 0.25 to 1.0 Cu-BrC, with the peak at 0.5 Cu-BrC. The dissolution rate of DCPD is greater than that of ß-TCP by a factor of 22, so the increase in DCPD phase intensity between 0.25 and 0.5 Cu-BrC may have contributed to the increase in setting time between the two [66]. This does not account for the extreme increase in setting time between 0.5 and 1.0 Cu-BrC, but as discussed earlier, the lattice shrinkage caused by the substitution of smaller Cu ions for the larger Ca ions also contributes to the increase in setting time.

When conducting compressive strength testing, the 1.0 Cu-BrC samples were visibly deteriorated compared to the other samples. The setting time was measured last and gave some insight into this deterioration. As shown in Figure 23, the initial setting time of 1.0 Cu-BrC was 14.67 minutes, and the final setting time was 51.17 minutes. Throughout the experiment, samples were transferred to the 37 °C environment to complete the setting time approximately 10 minutes after the cement was poured into the mold. After 1 hour, the samples were removed from the mold and transferred to PBS to further complete setting. However, this amount of time is barely more than the calculated final setting time of the 1.0 Cu-BrC samples. Because of this, the samples may not have had enough time to complete the setting reactions. However, based on the trend observed in the compression testing, one might expect the 1.0 Cu-BrC samples to have decreased strength compared to samples with less amounts of Cu. A general increase in setting time can be observed as the amount of Cu increases. However, there is a significant increase when 1.0 wt. % Cu is added. This signifies that Cu addition reduces the ability of the cement to set in a timely fashion, which is a significant consideration for injectable bone substitute materials.

Taking into account the significant increase in setting time of 1.0 Cu-BrC compared to the other samples, the results of the compressive testing are clear. A slight decrease in strength between 0.5 and 1.0 Cu-TCP was expected, but because of the extended period of time required to complete the setting reaction for 1.0 Cu-TCP compared to the reduced amount of time that the samples were allowed to set, this more drastic decrease of compressive strength can also be expected. By observing the data, it can be postulated that the maximum compressive strength can be obtained by adding between 0–0.5 wt. % Cu to BrC, since the maximum observed compressive strength was at 0.25 wt. % Cu. Thus, Cu has the potential to increase compressive strength of BrC depending on dopant amount.

The importance of the presence of Cu in the body as an essential trace element has been well documented, as has its toxicity on cellular and macro levels. Toxicity at a cellular level is often attributed to the breakdown of DNA strands by reactive oxygen species (ROS), which are created by Cu ions [133]. On a macro level, Cu toxicity can cause intestinal cramps, nausea, and decreased liver function [114]. In contrast, deficiency of Cu can lead to anemia and cardiomyopathy [111,114]. Cellular studies have shown an increase in VEGF secretion by mesenchymal stem cells with the addition of Cu to bioglass scaffolds and show no toxicity up to 1 wt. % Cu addition [135]. Wu et al. corroborate these findings and further show an increase of ALP, OCN, and OPN secretion in a dose-dependent manner, though at higher Cu concentrations cell toxicity was observed [116]. Many other studies have indicated similar results regarding VEGF and other osteoinductive markers, and similar results were reported previously [19–21]. This study observed osteogenic gene expression similar to previous observations, with a few notable differences.

Herein, a significant decrease in proliferation was observed with the addition of Cu dopant in a nearly linear dose-dependent manner at all kinetics. In an earlier study with ß-TCP scaffolds, relative OB proliferation was nearly equal for pure and 0.25 wt. % Cu scaffolds, whereas this study observed a significant decrease in relative proliferation at all concentrations of Cu. This highlights the difference in how cells react to various scaffolds, as all cellular procedures were constant between experiments.

At the day 3 time point, relative proliferation of 1.0 Cu-BrC was just over 20%, and at day 7 it was just under 40%. A similar trend was observed for 0.25 and 0.5 Cu-BrC, which may explain why all gene expressions except IL-17, RANKL, and OCN were almost negligible at day 7. These three genes all had relatively small gene expression at day 1, whereas at later time points they had exponentially more expression. RANKL expression for all Cu-doped samples was greater than 200,000% relative expression.

In a similar manner, IL-17 expression for 1.0 Cu-BrC at the latest kinetic was over 1,000,000% of relative IL-17 expression, and all doped samples were greater than 500,000%. IL-17 has been linked to increased expression of ALP, but that trend was not observed in this study [44]. Doped sample expression of ALP was increased at early time points but steadily decreased at later kinetics. At day 7, ALP expression for all doped samples was less than that of pure BrC. However, ALP is known as an early indicator of osteoblast differentiation and cellular activity, so lower expression at later kinetics when proliferation was decreased can be expected [129].

IL-17 is also often associated with the production of other proinflammatory cytokines such as IL-6 and TNF-α and has been linked to the expression of RANKL [43]. It seems that IL-17 can enhance bone regeneration but also play a role in osteoclastogenesis and the expression of inflammatory cytokines [43–45]. There does seem to be a link between the increase in IL-17 expression and the increase in RANKL expression at later kinetics, though there may be other factors involved.

The expression of IL-6 did not follow the pattern of IL-17 expression; IL-6 expression increased in a dose-dependent manner at the first time point, but expression slowly decreased until at the latest kinetic, and almost no IL-6 expression was observed with doped samples, compared to increased expression of IL-6 by the pure BrC at that time. IL-6 has been linked to osteoarthritis, osteoclastogenesis, and ECM mineralization and is a proinflammatory cytokine [38,39,41]. Cu may inhibit the expression of IL-6 at later kinetics, as the increase in expression of other osteoclastogenesis markers and proinflammatory cytokines was observed.

Similar to IL-6, TNF-α is a proinflammatory cytokine and is linked to osteoclastogenesis and inflammatory bone diseases [46,151]. It also inhibits expression of COLA-1 and OCN, and reduces the mineralization of the matrix [46,47]. TNF-α expression increased in a dose-dependent manner at the earliest time point, after which expression decreased for all doped samples compared to pure BrC, which suggests that at later kinetics Cu dopant had a therapeutic effect on reduction of this inflammatory cytokine.

To regulate osteoclastogenesis, OPG acts as a decoy receptor to RANKL, which binds to OPG instead of receptor activator of nuclear factor κ-ß (RANK) [19,24]. This inhibits the formation of osteoclasts and thus reduces bone resorption. Mice studies have shown that an overabundance of OPG expression results in osteopetrosis, whereas osteoporosis occurs with a lack of OPG [25]. In addition, RANKL and OPG expression have an inverse relationship, so increases in expression of RANKL are linked to decreases in expression of OPG [19]. There is clearly such an inverse relationship present in the data gathered in this experiment, as at later kinetics when RANKL expression significantly increased, relative OPG expression decreased. At the first time point, Cu-doped samples had a much greater OPG expression compared to pure BrC, and the same trend was present to a lesser degree at the second time point. The OPG expression at the final kinetic for all doped samples was significantly reduced compared to pure BrC at the final time point. This suggests a trend towards favorable conditions for osteoclastogenesis because of the increased IL-17 and RANKL expression combined with this decrease in OPG expression.

The metabolic activity of bone can be indicated by the gene OCN, the expression of which also indicates bone formation [49]. OCN is secreted solely by osteoblasts and bonds well with the hydroxyapatite in bone, helping to ensure mineralization [50,51]. It is secreted once the osteoblasts are mature, which is why an increase in OCN expression is seen at later kinetics. The highest levels of OCN expressed by Cu-doped samples occurred at day 3, whereas the highest expression of OCN for the undoped samples occurred at day 7. This could indicate that osteoblast cells cultured in the presence of Cu mature more rapidly than those cultured on pure BrC scaffolds. The increased expression of OCN at later kinetics on doped samples compared to the pure sample suggests that the presence of Cu does enhance osteoblast expression of OCN.

While OCN is one of the main noncollagenous proteins found in bone, collagen is by far the most abundant protein. Combined with COLA-2, COLA-1 produces the fibril-forming type 1 collagen, which is essential to the mineralization of the bone matrix, and it is also considered a marker of osteoblast differentiation and ALP production [48]. At early kinetics, a large increase was seen in COLA-1 production by doped samples in a dose-dependent manner, though at the final time point all expression of COLA-1 decreased. This, combined with a low expression of TNF-α at later kinetics and a high expression of OCN at early kinetics, suggests favorable bone matrix mineralization trends with the presence of Cu.

Angiogenesis and osteogenesis are closely related processes, and both are essential for healthy bone growth. The vascularization of bone ensures that blood can flow and provide oxygen to the bone. VEGF is an indicator of blood vessel growth and the ossification of bone and is mostly expressed during mineralization [33,34,36]. Thus, the increase in expression of VEGF at early time points for Cu-doped samples may indicate earlier mineralization compared to pure samples and again suggest a more rapid maturation of osteoblasts cultured in the presence of Cu. Reduction of VEGF expression at the latest kinetic for Cu-doped samples compared to pure BrC could occur because of the later maturation of osteoblast cells cultured on the pure BrC samples.

3.4.2 Co-BrC Discussion

The Co ionic radius is 0.074 nm, and it substitutes in the Ca^{2+} site in CaP ceramics. As a result of its smaller size compared to Ca^{2+} (0.099 nm), the substitution is accompanied by lattice shrinkage and enhances its stability, which, in turn, results in a slower dissolution rate. The XRD results herein show that the ß-TCP/DCPD (JCPDS No. 09-0077) ratio (calculated from the height of peaks with 100% intensity for ß-TCP and DCPD at $2\Theta = 31.1°$ and 21°, respectively) is increasing with the addition of dopants from 1.10 to 1.56, 1.68, and 2.02 for BrC, 0.25 Co-BrC, 0.5 Co-BrC, and 1.0 Co-BrC, respectively [106]. These results prove that the stability of TCP decreases the dissolution rate and, as a result, decreases the BrC formation.

Dissolution of precursors or precipitation of DCPD resulted in a prolonged setting reaction and in enhanced compressive strength in the Si-doped BrC system [87] and in the Cu-doped BrC system reported earlier. In this Co-BrC system, the setting time decreased slightly for low dopant amounts of Co, though at higher dopant amounts there was an increase in both initial and final setting times. This most likely occurs because of the increase in ß-TCP dissolution rate due to the formation of DCPD and the inhibited DCPD precipitation due to the presence of ß-TCP.

In this study, the Co dopants were added to TCP precursors prior to calcination. An alternative method for adding Co dopants that was attempted was to add corresponding $CoCl_2$ salt dopant amounts to the PEG-H_2O mixture, which was then mixed with pure powder. The samples were formed, but while the setting reactions were completed in PBS solution, the dopant began to leach out of the samples as shown in Figure 28. Therefore it was determined that, for all samples, dopant should be added to the TCP precursors.

Figure 28. $CoCl_2$ leached out of samples.

To evaluate the effects of Co and its concentration in BrC on osteosarcoma cell proliferation, the *in vitro* interaction between the cells and samples was investigated under both normoxic and hypoxic conditions. Co is a vital element in DNA synthesis, and its role as an antibacterial element is reported in reference [152]. Nevertheless, high concentrations of Co can cause toxicity in living cells [153]. Current results show that although there was a modest (20%) increase in MG-63 cell growth on pure BrC under hypoxia compared with normoxia, this increase did not reach statistical significance. Furthermore, the presence of Co at different concentrations did not affect MG-63 cell growth on BrC under normoxic or hypoxic conditions. These results are interesting because a previous study found that adding cobalt ions directly to the cell culture medium reduced the viability of osteoblasts and osteosarcoma cells in 2D culture [154]. However, the data shown in this study represent the 3D culture condition using a scaffold. Therefore, a comprehensive analysis of the differences between 2D and 3D cell culture models would aid in understanding the effects of Co and other additives to 3D cell culture systems. On the other hand, Zhang et al. found that the addition of Co to TCP at concentrations of 2 and 5 mol. % does not result in cytotoxicity in human bone marrow mesenchymal stem cells [142]. This proves that although the Co shows toxicity to some cell lines, its interaction with different cell lines in various systems should be evaluated [142].

Because hypoxia induces the expression of HIF-1α, this study examined HIF-1α expression by qPCR in MG-63 cells cultured on Co-BrC. Consistent with previous studies [141,142], MG-63 cells cultured on pure-BrC disks under hypoxic conditions significantly upregulated the expression of HIF-1α ($p = 0.0079$; Figure 27) [155]. The transcription factor GLI2 has been shown to be induced under hypoxic conditions. Furthermore, GLI2 has been shown to be upregulated in osteosarcoma tumor samples from patients, correlated with a poor prognosis, and its genetic inhibition results in a reduction in cell growth and survival [156–159]. Therefore, the GLI2 expression in the BrC model system was examined. Consistent with previous studies, the expression of GLI2 is induced in MG-63 cells cultured under hypoxic conditions on pure BrC ($p = 0.0002$; Figure 27).

Next the effect of Co on HIF-1α and GLI2 expression was examined. It was found that the presence of Co ions did not affect HIF-1α expression under normoxic conditions. Under hypoxic conditions, only the low dose of Co (0.25 wt. %) statistically reduced HIF-1α expression. Similarly, the addition of Co had no effect on GLI2 expression under normoxia. Nevertheless, under hypoxic conditions, the Co-BrC (1 wt. %) significantly reduced hypoxia-induced GLI2

expression (Figure 27). Taken together, these data suggest that in 3D cultures using Co-BrC, the addition of Co may reduce hypoxia-induced modulation of HIF-1α and GLI2 expression. Both hypoxia [145,160,161] and GLI2 [118,162] have been shown to induce inflammatory cytokine genes. Therefore, Co may indirectly reduce inflammation by regulating the expression of two proteins that regulate inflammation. Inflammation has been shown to promote tumorigenesis [163], and it facilitates osteosarcoma cell growth [164]; therefore, this 3D Co-BrC model system may provide therapeutic benefit for osteosarcoma by reducing hypoxia-induced gene expression.

3.5 Conclusion

In this work, the effect of Cu and Co dopants on the physical and biological characteristics of BrC was studied. The addition of up to 0.25 wt. % Cu was found to enhance the compressive strength of BrC samples. DCPD precipitation was clearly inhibited with the addition of Cu and Co, and as a result the setting time increased with increasing Cu and Co content. Cu also reduced the expression of inflammatory markers and enhanced the expression of osteogenic markers such as VEGF, while Co inhibited the expression of proinflammatory HIF-1α and GLI2 under hypoxia. No cytotoxicity was observed for MG-63 osteosarcoma cells under hypoxia or normoxia with the addition of Co dopant, though reduced proliferation was observed for OB cells with all amounts of Cu dopant.

CHAPTER 4 SUMMARY AND FUTURE WORK

4.1 Summary

Because of the prominence of diseases such as osteoporosis and arthritis, which affect people worldwide and even in outer space, the biology, engineering, materials science, and medical communities are actively studying various biomaterials that may be utilized as bone substitute materials. Calcium phosphates are among the materials studied and are promising because of their compositional similarity to bone, their resorption behavior, and their ability to be used in different forms. Calcium phosphates are naturally osteoconductive, but they lack osteoinductivity, or the ability to induce *de novo* bone formation. Because of this, various methods are utilized to stimulate bone formation in conjunction with these CaP materials, including incorporating growth factors and trace amounts of essential elements. By integrating metal ions into the CaP materials, the physical and mechanical properties of the materials can also be modified.

In this study, trace amounts of Cu and Co were incorporated into tricalcium phosphate and brushite cement calcium phosphate materials in an effort to quantify the biological and physical impact of the incorporation of these materials. An excess of these metals can be toxic to the body or have an adverse effect on the physical and mechanical properties, so various trace amounts were utilized.

As anticipated, the incorporation of Cu and Co into TCP and BrC caused changes in the microstructure and phase diagrams of the materials. The density, setting time, and compressive

strength were also altered. The compressive strength of Cu-BrC increased with 0.25 Cu dopant but decreased with increasing amounts of Cu. The initial and final setting times of Cu- and Co-doped BrC increased with increasing amounts of dopant, and a significant increase in setting time was observed between 0.5 and 1.0 Cu-BrC. Decreasing amounts of DCPD precipitation were observed in the XRD data for BrC with incorporation of dopants. The open porosity of TCP samples was impacted less by sintering temperature when Cu dopants were present. In addition, the α-TCP phase was inhibited from forming by the incorporation of Cu into TCP samples.

Biologically, the incorporation of Cu and Co into samples resulted in both positive and negative osteoinductive impacts. The expression of gene markers is commonly used to quantify osteoinduction, and several of those markers were studied herein. In the two Cu studies, IL-17, IL-6, TNF-α, RANKL, OPG, ALP-1, VEGF, COLA-1, and OCN expressions were observed. IL-17, IL-6, and TNF-α are proinflammatory gene markers, though they have beneficial roles as well. IL-17 expression increased in both studies, though IL-6 and TNF-α expression decreased at later kinetics, suggesting that Cu plays a therapeutic role in reduction of inflammation. The early increase in expression of ALP-1 and VEGF, and the later increase of expression in OCN indicates that Cu plays a beneficial role in osteoinduction in osteoblasts for BrC and TCP.

The incorporation of Co into BrC samples reduced the expression of HIF-1α and GLI2 under hypoxic conditions, which again signifies that Co has an anti-inflammatory therapeutic effect on MG-63 osteosarcoma cells. In addition, no cytotoxicity was observed with doped samples compared to MG-63 proliferation on pure-BrC samples. These positive effects of Cu and Co on the osteoinductive markers and the reduction in expression of proinflammatory markers suggest that further investigation and laboratory testing should be conducted on these two trace elements.

4.2 Future Work

The author recommends continued research on BrC and TCP calcium phosphates as bone substitute materials. The compressive strength of Cu-TCP and Co-BrC were not considered in this study, but should be investigated. In addition, therapeutic effects were observed for all dopant amounts of Co, so increased wt. % of Co dopant may be considered. The surface morphologies should be further considered for the Cu-doped materials as well.

Co-BrC had therapeutic effects on reducing HIF-1α and GLI2 expression, but no qPCR was conducted to quantify the effects of Co addition on other osteoinductive markers. Further research should be conducted in considering those markers. In addition, Co-TCP was not considered and should be investigated as a bone substitute material.

In vitro studies were conducted in the research presented herein, but further work should include *in vivo* studies using rabbits and rats in a laboratory setting. Histological results offer further insight into the effects of dopants on tissue and a more complete picture of the ramifications of utilizing potentially toxic metals. Because of the promising initial results presented herein, *in vivo* studies should be pursued.

Finally, the incorporation of other trace elements, such as Chromium (Cr), should continue to be studied, as should alternative sample fabrication methods. Work has begun to control the

porosity of TCP samples through the use of substances such as naphthalene, which can be incorporated in controlled particle sizes and then evaporated using low-heat furnaces. The utilization of such porous samples, and the sequential incorporation of dopants into the samples, could further enhance the osteoinductive capacity of TCP and increase its ability to bond with bone.

REFERENCES

[1] Trotter, M., "A Preliminary Study of Estimation of Weight of the Skeleton," Am. J. Phys. Anthropol., 12(4), 1954, pp. 537–552.

[2] Rho, J. Y., Kuhn-Spearing, L., and Zioupos, P., "Mechanical Properties and the Hierarchical Structure of Bone," Med. Eng. Phys., 20(2), 1998, pp. 92–102.

[3] Ascenzi, A., and Bonucci, E., "The Tensile Properties of Single Osteons," Anat. Rec., 158(4), 1967, pp. 375–386.

[4] Ascenzi, A., and Bonucci, E., "The Compressive Properties of Single Osteons," Anat. Rec., 161(3), 1968, pp. 377–391.

[5] Ascenzi, A., Baschieri, P., and Benvenuti, A., "The Bending Properties of Single Osteons," J. Biomech., 23(8), 1990, pp. 763–771.

[6] Ascenzi, A., Baschieri, P., and Benvenuti, A., "The Torsional Properties of Single Selected Osteons," J. Biomech., 27(7), 1994, pp. 875–884.

[7] "Bone Anatomy Cortex The Microstructural and Biomechanical Development of The Condylar," Hum. Anat. Body [Online]. Available: https://www.anatomylibrary99.com/bone-anatomy-cortex/bone-anatomy-cortex-the-microstructural-and-biomechanical-development-of-the-condylar/. [Accessed: 23-Feb-2018].

[8] Black, J., and Hastings, G., eds., *Handbook of Biomaterial Properties*, Springer US, 1998.

[9] Fung, Y. C., *Biomechanics: Mechanical Properties of Living Tissues*, Springer-Verlag, New York, 1993.

[10] Pal, S., *Design of Artificial Human Joints & Organs*, Springer US, 2014.

[11] Aubin, J., and Lian, J., "Bone Formation: Maturation and Functional Activities of Osteoblast Lineage Cells," *Primer on the Metabolic Bone Diseases and Disorders of Mineral Metabolism*, American Society for Bone and Mineral Research, Washington, 2006, pp. 20–29.

[12] Komori, T., Yagi, H., Nomura, S., Yamaguchi, A., Sasaki, K., Deguchi, K., Shimizu, Y., Bronson, R. T., Gao, Y. H., Inada, M., Sato, M., Okamoto, R., Kitamura, Y., Yoshiki, S., and Kishimoto, T., "Targeted Disruption of Cbfa1 Results in a Complete Lack of Bone Formation Owing to Maturational Arrest of Osteoblasts," Cell, 89(5), 1997, pp. 755–764.

[13] Nakamura, H., "Morphology, Function, and Differentiation of Bone Cells," J. Hard Tissue Biol., 16, 2007, pp. 15–22.

[14] Rutkovskiy, A., Stensløkken, K.-O., and Vaage, I. J., “Osteoblast Differentiation at a Glance,” Med. Sci. Monit. Basic Res., 22, 2016, pp. 95–106.

[15] Knothe Tate, M. L., Adamson, J. R., Tami, A. E., and Bauer, T. W., “The Osteocyte,” Int. J. Biochem. Cell Biol., 36(1), 2004, pp. 1–8.

[16] Nampei, A., Hashimoto, J., Hayashida, K., Tsuboi, H., Shi, K., Tsuji, I., Miyashita, H., Yamada, T., Matsukawa, N., Matsumoto, M., Morimoto, S., Ogihara, T., Ochi, T., and Yoshikawa, H., “Matrix Extracellular Phosphoglycoprotein (MEPE) Is Highly Expressed in Osteocytes in Human Bone,” J. Bone Miner. Metab., 22(3), 2004, pp. 176–184.

[17] Ypey, D. L., Weidema, A. F., Höld, K. M., Van der Laarse, A., Ravesloot, J. H., Van Der Plas, A., and Nijweide, P. J., “Voltage, Calcium, and Stretch Activated Ionic Channels and Intracellular Calcium in Bone Cells,” J. Bone Miner. Res., 7 (S2), 1992, pp. S377-387.

[18] “Bone | Boundless Biology” [Online]. Available: https://courses.lumenlearning.com/boundless-biology/chapter/bone/. [Accessed: 23-Feb-2018].

[19] Boyce, B. F., and Xing, L., “Biology of RANK, RANKL, and Osteoprotegerin,” Arthritis Res. Ther., 9 Suppl 1, 2007, p. S1.

[20] Udagawa, N., Takahashi, N., Yasuda, H., Mizuno, A., Itoh, K., Ueno, Y., Shinki, T., Gillespie, M. T., Martin, T. J., Higashio, K., and Suda, T., “Osteoprotegerin Produced by Osteoblasts Is an Important Regulator in Osteoclast Development and Function,” Endocrinology, 141(9), 2000, pp. 3478–3484.

[21] Osta, B., “Effects of Interleukine-17A (Il-17A) and Tumor Necrosis Factor Alpha (TNF-α) on Osteoblastic Differentiation,” Université Claude Bernard - Lyon 1, 2014.

[22] Teitelbaum, S. L., and Ross, F. P., “Genetic Regulation of Osteoclast Development and Function,” Nat. Rev. Genet., 4(8), 2003, pp. 638–649.

[23] Imai, Y., Youn, M.-Y., Inoue, K., Takada, I., Kouzmenko, A., and Kato, S., “Nuclear Receptors in Bone Physiology and Diseases,” Physiol. Rev., 93(2), 2013, pp. 481–523.

[24] Kohli, S. S., and Kohli, V. S., “Role of RANKL-RANK/Osteoprotegerin Molecular Complex in Bone Remodeling and Its Immunopathologic Implications,” Indian J. Endocrinol. Metab., 15(3), 2011, pp. 175–181.

[25] Kong, Y.-Y., Boyle, W. J., and Penninger, J. M., “Osteoprotegerin Ligand: A Common Link between Osteoclastogenesis, Lymph Node Formation and Lymphocyte Development,” Immunol. Cell Biol., 77(2), 1999, pp. 188–193.

[26] Anh, D. J., Dimai, H. P., Hall, S. L., and Farley, J. R., “Skeletal Alkaline Phosphatase Activity Is Primarily Released From Human Osteoblasts in an Insoluble Form, and the Net Release Is Inhibited by Calcium and Skeletal Growth Factors,” Calcif. Tissue Int., 62(4), 1998, pp. 332–340.

[27] Golub, E., and Boesze-Battaglia, K., “The Role of Alkaline Phosphatase in Mineralization,” Curr. Opin. Orthop., (18), 2007, pp. 444–448.

[28] Masrour Roudsari, J., and Mahjoub, S., "Quantification and Comparison of Bone-Specific Alkaline Phosphatase with Two Methods in Normal and Paget's Specimens," Casp. J. Intern. Med., 3(3), 2012, pp. 478–483.

[29] Kirkham, G. R., and Cartmell, S. H., "Genes and Proteins Involved in the Regulation of Osteogenesis," *Topics in Tissue Engineering*, Oulu University, Oulu, Finland, 2007.

[30] Street, J., Bao, M., deGuzman, L., Bunting, S., Peale, F. V., Ferrara, N., Steinmetz, H., Hoeffel, J., Cleland, J. L., Daugherty, A., van Bruggen, N., Redmond, H. P., Carano, R. A. D., and Filvaroff, E. H., "Vascular Endothelial Growth Factor Stimulates Bone Repair by Promoting Angiogenesis and Bone Turnover," Proc. Natl. Acad. Sci. U. S. A., 99(15), 2002, pp. 9656–9661.

[31] Hu, K., and Olsen, B. R., "Osteoblast-Derived VEGF Regulates Osteoblast Differentiation and Bone Formation during Bone Repair," J. Clin. Invest., 126(2), 2016, pp. 509–526.

[32] Maes, C., and Carmeliet, G., *Vascular and Nonvascular Roles of VEGF in Bone Development*, Landes Bioscience, 2013.

[33] Gerber, H. P., Vu, T., M. Ryan, A., Kowalski, J., Werb, Z., and Ferrara, N., "Gerber, HP, Vu, TH, Ryan, AM, Kowalski, J, Werb, Z and Ferrara, N. VEGF Couples Hypertrophic Cartilage Remodeling, Ossification and Angiogenesis during Endochondral Bone Formation, Nat. Med., 5, 1999, pp. 623–8.

[34] Coultas, L., Chawengsaksophak, K., and Rossant, J., "Endothelial Cells and VEGF in Vascular Development," Nature, 438(7070), 2005, pp. 937–945.

[35] Fiedler, J., Leucht, F., Waltenberger, J., Dehio, C., and Brenner, R. E., "VEGF-A and PlGF-1 Stimulate Chemotactic Migration of Human Mesenchymal Progenitor Cells," Biochem. Biophys. Res. Commun., 334(2), 2005, pp. 561–568.

[36] Deckers, M. M., Karperien, M., van der Bent, C., Yamashita, T., Papapoulos, S. E., and Löwik, C. W., "Expression of Vascular Endothelial Growth Factors and Their Receptors During Osteoblast Differentiation," Endocrinology, 141(5), 2000, pp. 1667–1674.

[37] Yang, Y.-Q., Tan, Y.-Y., Wong, R., Wenden, A., Zhang, L.-K., and Rabie, A. B. M., "The Role of Vascular Endothelial Growth Factor in Ossification," Int. J. Oral Sci., 4(2), 2012, pp. 64–68.

[38] Axmann, R., Böhm, C., Krönke, G., Zwerina, J., Smolen, J., and Schett, G., "Inhibition of Interleukin-6 Receptor Directly Blocks Osteoclast Formation in Vitro and in Vivo," Arthritis Rheum., 60(9), 2009, pp. 2747–2756.

[39] Blanchard, F., Duplomb, L., Baud'huin, M., and Brounais, B., "The Dual Role of IL-6-Type Cytokines on Bone Remodeling and Bone Tumors," Cytokine Growth Factor Rev., 20(1), 2009, pp. 19–28.

[40] Nasi, S., So, A., Combes, C., Daudon, M., and Busso, N., "Interleukin-6 and Chondrocyte Mineralisation Act in Tandem to Promote Experimental Osteoarthritis," Ann. Rheum. Dis., 75(7), 2016, pp. 1372–1379.

[41] Stack, J., and McCarthy, G., “Basic Calcium Phosphate Crystals and Osteoarthritis Pathogenesis: Novel Pathways and Potential Targets,” Curr. Opin. Rheumatol., 28(2), 2016, pp. 122–126.

[42] Jin, W., and Dong, C., “IL-17 Cytokines in Immunity and Inflammation,” Emerg. Microbes Infect., 2(9), 2013, p. e60.

[43] Lee, Y., “The Role of Interleukin-17 in Bone Metabolism and Inflammatory Skeletal Diseases,” BMB Rep., 46(10), 2013, pp. 479–483.

[44] Croes, M., Öner, F. C., van Neerven, D., Sabir, E., Kruyt, M. C., Blokhuis, T. J., Dhert, W. J. A., and Alblas, J., “Proinflammatory T Cells and IL-17 Stimulate Osteoblast Differentiation,” Bone, 84, 2016, pp. 262–270.

[45] Won, H. Y., Lee, J.-A., Park, Z. S., Song, J. S., Kim, H. Y., Jang, S.-M., Yoo, S.-E., Rhee, Y., Hwang, E. S., and Bae, M. A., “Prominent Bone Loss Mediated by RANKL and IL-17 Produced by CD4+ T Cells in TallyHo/JngJ Mice,” PLOS ONE, 6(3), 2011, p. e18168.

[46] Abbas, S., Zhang, Y.-H., Clohisy, J. C., and Abu-Amer, Y., “Tumor Necrosis Factor-Alpha Inhibits Pre-Osteoblast Differentiation through Its Type-1 Receptor,” Cytokine, 22(1–2), 2003, pp. 33–41.

[47] Gilbert, L., He, X., Farmer, P., Boden, S., Kozlowski, M., Rubin, J., and Nanes, M. S., “Inhibition of Osteoblast Differentiation by Tumor Necrosis Factor-Alpha,” Endocrinology, 141(11), 2000, pp. 3956–3964.

[48] Jikko, A., Harris, S. E., Chen, D., Mendrick, D. L., and Damsky, C. H., “Collagen Integrin Receptors Regulate Early Osteoblast Differentiation Induced by BMP-2,” J. Bone Miner. Res., 14(7), 1999, pp. 1075–1083.

[49] Cantatore, F. P., Corrado, A., Grano, M., Quarta, L., Colucci, S., and Melillo, N., “Osteocalcin Synthesis by Human Osteoblasts from Normal and Osteoarthritic Bone After Vitamin D3 Stimulation,” Clin. Rheumatol., 23(6), 2004, pp. 490–495.

[50] Sila-Asna, M., Bunyaratvej, A., Maeda, S., Kitaguchi, H., and Bunyaratavej, N., “Osteoblast Differentiation and Bone Formation Gene Expression in Strontium-Inducing Bone Marrow Mesenchymal Stem Cell,” Kobe J. Med. Sci., 53(1–2), 2007, pp. 25–35.

[51] Hoang, Q. Q., Sicheri, F., Howard, A. J., and Yang, D. S. C., “Bone Recognition Mechanism of Porcine Osteocalcin from Crystal Structure,” Nature, 425(6961), 2003, pp. 977–980.

[52] Ducy, P., Desbois, C., Boyce, B., Pinero, G., Story, B., Dunstan, C., Smith, E., Bonadio, J., Goldstein, S., Gundberg, C., Bradley, A., and Karsenty, G., “Increased Bone Formation in Osteocalcin-Deficient Mice,” Nature, 382(6590), 1996, pp. 448–452.

[53] Wang, Y., Wan, C., Deng, L., Liu, X., Cao, X., Gilbert, S. R., Bouxsein, M. L., Faugere, M.-C., Guldberg, R. E., Gerstenfeld, L. C., Haase, V. H., Johnson, R. S., Schipani, E., and Clemens, T. L., “The Hypoxia-Inducible Factor Alpha Pathway Couples Angiogenesis to Osteogenesis During Skeletal Development,” J. Clin. Invest., 117(6), 2007, pp. 1616–1626.

[54] Wan, C., Shao, J., Gilbert, S. R., Riddle, R. C., Long, F., Johnson, R. S., Schipani, E., and Clemens, T. L., "Role of HIF-1alpha in Skeletal Development," Ann. N. Y. Acad. Sci., 1192, 2010, pp. 322–326.

[55] Fernández-Torres, J., Hernández-Díaz, C., Espinosa-Morales, R., Camacho-Galindo, J., Galindo-Sevilla, N. del C., López-Macay, Á., Zamudio-Cuevas, Y., Martínez-Flores, K., Santamaría-Olmedo, M. G., Pineda, C., Granados, J., Martínez-Nava, G. A., Gutiérrez, M., and López-Reyes, A. G., "Polymorphic Variation of Hypoxia Inducible Factor-1 A (HIF1A) Gene Might Contribute to the Development of Knee Osteoarthritis: A Pilot Study," BMC Musculoskelet. Disord., 16, 2015.

[56] Looker, A., Isfahani, N., Fan, B., and Shepherd, J., 2017, "FRAX-Based Estimates of 10-Year Probability of Hip and Major Osteoporotic Fracture Among Adults Aged 40 and Over: United States, 2013 and 2014," www.CDC.gov [Online]. Available: https://www.cdc.gov/nchs/data/nhsr/nhsr103.pdf.

[57] Hootman, J. M., Helmick, C. G., Barbour, K. E., Theis, K. A., and Boring, M. A., "Updated Projected Prevalence of Self-Reported Doctor-Diagnosed Arthritis and Arthritis-Attributable Activity Limitation Among US Adults, 2015-2040," Arthritis Rheumatol. Hoboken NJ, 68(7), 2016, pp. 1582–1587.

[58] Murphy, L., Bolen, J., Helmick, C., and Brady, T., 2017, "Comorbidities Are Very Common Among People With Arthritis," www.CDC.gov [Online]. Available: https://www.cdc.gov/arthritis/data_statistics/comorbidities.htm.

[59] Sibonga, J. D., "Spaceflight-Induced Bone Loss: Is There an Osteoporosis Risk?," Curr. Osteoporos. Rep., 11(2), 2013, pp. 92–98.

[60] "Slideshow: A Visual Guide to Osteoporosis," WebMD [Online]. Available: https://www.webmd.com/osteoporosis/ss/slideshow-osteoporosis-overview. [Accessed: 23-Feb-2018].

[61] Drummond, J., Tran, P., and Fary, C., "Metal-on-Metal Hip Arthroplasty: A Review of Adverse Reactions and Patient Management," J. Funct. Biomater., 6(3), 2015, pp. 486–499.

[62] Anderson, J. M., Rodriguez, A., and Chang, D. T., "Foreign Body Reaction to Biomaterials," Semin. Immunol., 20(2), 2008, pp. 86–100.

[63] Nouri, A., "Novel Metal Structures Through Powder Metallurgy for Biomedical Applications," Deakin University, 2008.

[64] Hannink, G., and Arts, J. J. C., "Bioresorbability, Porosity and Mechanical Strength of Bone Substitutes: What Is Optimal for Bone Regeneration?," Injury, 42, 2011, pp. S22–S25.

[65] Boanini, E., Gazzano, M., and Bigi, A., "Ionic Substitutions in Calcium Phosphates Synthesized at Low Temperature," Acta Biomater., 6(6), 2010, pp. 1882–1894.

[66] Ravaglioli, A., and Krajewski, A., *Bioceramics: Materials. Properties. Applications*, Springer, 1991.

[67] Welch, J. H., and Gutt, W., "High-Temperature Studies of the System Calcium Oxide–phosphorus Pentoxide," J. Chem. Soc. Resumed, (4), 1961, pp. 4442–4444.

[68] LeGeros, R. Z., "Calcium Phosphate-Based Osteoinductive Materials," Chem. Rev., 108(11), 2008, pp. 4742–4753.

[69] Elliott, J. C., Structure and Chemistry of the Apatites and Other Calcium Orthophosphates, Elsevier, 2013.

[70] García, F., Ortega, A., Domingo, J. L., and Corbella, J., "Accumulation of Metals in Autopsy Tissues of Subjects Living in Tarragona County, Spain," J. Environ. Sci. Health Part A Tox. Hazard. Subst. Environ. Eng., 36(9), 2001, pp. 1767–1786.

[71] Cheng, L., Ye, F., Yang, R., Lu, X., Shi, Y., Li, L., Fan, H., and Bu, H., "Osteoinduction of Hydroxyapatite/Beta-Tricalcium Phosphate Bioceramics in Mice with a Fractured Fibula," Acta Biomater., 6(4), 2010, pp. 1569–1574.

[72] Bose, S., Fielding, G., Tarafder, S., and Bandyopadhyay, A., "Understanding of Dopant-Induced Osteogenesis and Angiogenesis in Calcium Phosphate Ceramics," Trends Biotechnol., 31(10), 2013, pp. 594–605.

[73] Samavedi, S., Whittington, A. R., and Goldstein, A. S., "Calcium Phosphate Ceramics in Bone Tissue Engineering: A Review of Properties and Their Influence on Cell Behavior," Acta Biomater., 9(9), 2013, pp. 8037–8045.

[74] Seeherman, H., and Wozney, J. M., "Delivery of Bone Morphogenetic Proteins for Orthopedic Tissue Regeneration," Cytokine Growth Factor Rev., 16(3), 2005, pp. 329–345.

[75] Takahashi, Y., Yamamoto, M., and Tabata, Y., "Enhanced Osteoinduction by Controlled Release of Bone Morphogenetic Protein-2 From Biodegradable Sponge Composed of Gelatin and Beta-Tricalcium Phosphate," Biomaterials, 26(23), 2005, pp. 4856–4865.

[76] Vahabzadeh, S., Bandyopadhyay, A., Bose, S., Mandal, R., and Nandi, S. K., "IGF-Loaded Silicon and Zinc Doped Brushite Cement: Physico-Mechanical Characterization and in Vivo Osteogenesis Evaluation," Integr. Biol. Quant. Biosci. Nano Macro, 7(12), 2015, pp. 1561–1573.

[77] Weir, M. D., and Xu, H. H. K., "Human Bone Marrow Stem Cell-Encapsulating Calcium Phosphate Scaffolds for Bone Repair," Acta Biomater., 6(10), 2010, pp. 4118–4126.

[78] Gérard, C., Bordeleau, L.-J., Barralet, J., and Doillon, C. J., "The Stimulation of Angiogenesis and Collagen Deposition by Copper," Biomaterials, 31(5), 2010, pp. 824–831.

[79] Pina, S., Vieira, S. I., Rego, P., Torres, P. M. C., da Cruz e Silva, O. A. B., da Cruz e Silva, E. F., and Ferreira, J. M. F., "Biological Responses of Brushite-Forming Zn- and ZnSr- Substituted Beta-Tricalcium Phosphate Bone Cements," Eur. Cell. Mater., 20, 2010, pp. 162–177.

[80] Li, X., Sogo, Y., Ito, A., Mutsuzaki, H., Ochiai, N., Kobayashi, T., Nakamura, S., Yamashita, K., and LeGeros, R. Z., "The Optimum Zinc Content in Set Calcium Phosphate Cement for Promoting Bone Formation in Vivo," Mater. Sci. Eng. C Mater. Biol. Appl., 29(3), 2009, pp. 969–975.

[81] Rude, R. K., Gruber, H. E., Wei, L. Y., and Frausto, A., "Immunolocalization of RANKL Is Increased and OPG Decreased During Dietary Magnesium Deficiency in the Rat," Nutr. Metab., 2, 2005, p. 24.

[82] Vahabzadeh, S., Tarafder, S., and Bose, S., "Osteoblast Differentiation in SrO and MgO Doped Tricalcium Phosphate; Gene Expression Study" [abstract]. In: Annual Meeting of the Society for Biomaterials. 2014 April 16-19. Denver, CO. Abstract no. 692.

[83] Guo, Y., Ren, L., Liu, C., Yuan, Y., Lin, X., Tan, L., Chen, S., Yang, K., and Mei, X., "Effect of Implantation of Biodegradable Magnesium Alloy on BMP-2 Expression in Bone of Ovariectomized Osteoporosis Rats," Mater. Sci. Eng. C Mater. Biol. Appl., 33(7), 2013, pp. 4470–4474.

[84] Vahabzadeh, S., Hack, V. K., and Bose, S., "Lithium-Doped β-Tricalcium Phosphate: Effects on Physical, Mechanical and in Vitro Osteoblast Cell-Material Interactions," J. Biomed. Mater. Res. B Appl. Biomater., 105(2), 2017, pp. 391–399.

[85] Han, P., Xu, M., Chang, J., Chakravorty, N., Wu, C., and Xiao, Y., "Lithium Release from β-Tricalcium Phosphate Inducing Cementogenic and Osteogenic Differentiation of Both hPDLCs and hBMSCs," Biomater. Sci., 2(9), 2014, pp. 1230–1243.

[86] Thorfve, A., Lindahl, C., Xia, W., Igawa, K., Lindahl, A., Thomsen, P., Palmquist, A., and Tengvall, P., "Hydroxyapatite Coating Affects the Wnt Signaling Pathway During Peri-Implant Healing in Vivo," Acta Biomater., 10(3), 2014, pp. 1451–1462.

[87] Vahabzadeh, S., Roy, M., and Bose, S., "Effects of Silicon on Osteoclast Cell Mediated Degradation, In Vivo Osteogenesis and Vasculogenesis of Brushite Cement," J. Mater. Chem. B Mater. Biol. Med., 3(46), 2015, pp. 8973–8982.

[88] Obata, A., and Kasuga, T., "Stimulation of Human Mesenchymal Stem Cells and Osteoblasts Activities in Vitro on Silicon-Releasable Scaffolds," J. Biomed. Mater. Res. A, 91(1), 2009, pp. 11–17.

[89] Li, H., and Chang, J., "Bioactive Silicate Materials Stimulate Angiogenesis in Fibroblast and Endothelial Cell Co-Culture System Through Paracrine Effect," Acta Biomater., 9(6), 2013, pp. 6981–6991.

[90] Reffitt, D. M., Ogston, N., Jugdaohsingh, R., Cheung, H. F. J., Evans, B. A. J., Thompson, R. P. H., Powell, J. J., and Hampson, G. N., "Orthosilicic Acid Stimulates Collagen Type 1 Synthesis and Osteoblastic Differentiation in Human Osteoblast-like Cells in Vitro," Bone, 32(2), 2003, pp. 127–135.

[91] Gaetke, L. M., and Chow, C. K., "Copper Toxicity, Oxidative Stress, and Antioxidant Nutrients," Toxicology, 189(1–2), 2003, pp. 147–163.

[92] Barceloux, D. G., "Copper," J. Toxicol. Clin. Toxicol., 37(2), 1999, pp. 217–230.

[93] Arredondo, M., and Núñez, M. T., "Iron and Copper Metabolism," Mol. Aspects Med., 26(4–5), 2005, pp. 313–327.

[94] D'Andrea, L. D., Romanelli, A., Di Stasi, R., and Pedone, C., "Bioinorganic Aspects of Angiogenesis," Dalton Trans. Camb. Engl. 2003, 39(33), 2010, pp. 7625–7636.

[95] Barralet, J., Gbureck, U., Habibovic, P., Vorndran, E., Gerard, C., and Doillon, C. J., "Angiogenesis in Calcium Phosphate Scaffolds by Inorganic Copper Ion Release," Tissue Eng. Part A, 15(7), 2009, pp. 1601–1609.

[96] Gbureck, U., Hoelzel, T., J. Doillon, C., Müller, F., and Barralet, J., "Direct Printing of Bioceramic Implants with Spatially Localized Angiogenic Factors," Adv. Mater., 19, 2007, pp. 795–800.

[97] Lauwerys, R., and Lison, D., "Health Risks Associated with Cobalt Exposure—an Overview," Sci. Total Environ., 150(1), 1994, pp. 1–6.

[98] Barceloux, D. G., "Cobalt," J. Toxicol. Clin. Toxicol., 37(2), 1999, pp. 201–206.

[99] Okamoto, S., and Eltis, L. D., "The Biological Occurrence and Trafficking of Cobalt," Metallomics, 3(10), 2011, pp. 963–970.

[100] Keegan, G. M., Learmonth, I. D., and Case, C. P., "Orthopaedic Metals and Their Potential Toxicity in the Arthroplasty Patient: A Review of Current Knowledge and Future Strategies," J. Bone Joint Surg. Br., 89(5), 2007, pp. 567–573.

[101] Mao, X., Wong, A. A., and Crawford, R. W., "Cobalt Toxicity—an Emerging Clinical Problem in Patients with Metal-on-Metal Hip Prostheses?," Med. J. Aust., 194(12), 2011, pp. 649–651.

[102] Inzana, J. A., Olvera, D., Fuller, S. M., Kelly, J. P., Graeve, O. A., Schwarz, E. M., Kates, S. L., and Awad, H. A., "3D Printing of Composite Calcium Phosphate and Collagen Scaffolds for Bone Regeneration," Biomaterials, 35(13), 2014, pp. 4026–4034.

[103] Rezwan, K., Chen, Q. Z., Blaker, J. J., and Boccaccini, A. R., "Biodegradable and Bioactive Porous Polymer/Inorganic Composite Scaffolds for Bone Tissue Engineering," Biomaterials, 27(18), 2006, pp. 3413–3431.

[104] Phipps, M. C., Clem, W. C., Grunda, J. M., Clines, G. A., and Bellis, S. L., "Increasing the Pore Sizes of Bone-Mimetic Electrospun Scaffolds Comprised of Polycaprolactone, Collagen I and Hydroxyapatite to Enhance Cell Infiltration," Biomaterials, 33(2), 2012, pp. 524–534.

[105] Espanol, M., Perez, R. A., Montufar, E. B., Marichal, C., Sacco, A., and Ginebra, M. P., "Intrinsic Porosity of Calcium Phosphate Cements and Its Significance for Drug Delivery and Tissue Engineering Applications," Acta Biomater., 5(7), 2009, pp. 2752–2762.

[106] Roy, M., DeVoe, K., Bandyopadhyay, A., and Bose, S., "Mechanical and In Vitro Biocompatibility of Brushite Cement Modified by Polyethylene Glycol," Mater. Sci. Eng. C Mater. Biol. Appl., 32(8), 2012, pp. 2145–2152.

[107] Zhang, J., Liu, W., Schnitzler, V., Tancret, F., and Bouler, J.-M., "Calcium Phosphate Cements for Bone Substitution: Chemistry, Handling and Mechanical Properties," Acta Biomater., 10(3), 2014, pp. 1035–1049.

[108] Rodríguez-Lorenzo, L. M., Vallet-Regí, M., and Ferreira, J. M. F., "Fabrication of Hydroxyapatite Bodies by Uniaxial Pressing from a Precipitated Powder," Biomaterials, 22(6), 2001, pp. 583–588.

[109] Cummings, H., Han, W., Vahabzadeh, S., and Elsawa, S. F., "Cobalt-Doped Brushite Cement: Preparation, Characterization, and In Vitro Interaction with Osteosarcoma Cells," JOM, 69(8), 2017, pp. 1348–1353.

[110] Bose, S., Tarafder, S., Banerjee, S. S., Davies, N. M., and Bandyopadhyay, A., "Understanding in Vivo Response and Mechanical Property Variation in MgO, SrO and SiO_2 Doped β-TCP," Bone, 48(6), 2011, pp. 1282–1290.

[111] Turski, M. L., and Thiele, D. J., "New Roles for Copper Metabolism in Cell Proliferation, Signaling, and Disease," J. Biol. Chem., 284(2), 2009, pp. 717–721.

[112] Kim, B.-E., Nevitt, T., and Thiele, D. J., "Mechanisms for Copper Acquisition, Distribution and Regulation," Nat. Chem. Biol., 4(3), 2008, pp. 176–185.

[113] Linder, M. C., *Biochemistry of Copper*, Springer Science & Business Media, 1991.

[114] Burch, R. E., Hahn, H. K., and Sullivan, J. F., "Newer Aspects of the Roles of Zinc, Manganese, and Copper in Human Nutrition," Clin. Chem., 21(4), 1975, p. 501–520.

[115] Harris, Z. L., Takahashi, Y., Miyajima, H., Serizawa, M., MacGillivray, R. T., and Gitlin, J. D., "Aceruloplasminemia: Molecular Characterization of This Disorder of Iron Metabolism," Proc. Natl. Acad. Sci. U. S. A., 92(7), 1995, pp. 2539–2543.

[116] Wu, C., Zhou, Y., Xu, M., Han, P., Chen, L., Chang, J., and Xiao, Y., "Copper-Containing Mesoporous Bioactive Glass Scaffolds with Multifunctional Properties of Angiogenesis Capacity, Osteostimulation and Antibacterial Activity," Biomaterials, 34(2), 2013, pp. 422–433.

[117] Ewald, A., Käppel, C., Vorndran, E., Moseke, C., Gelinsky, M., and Gbureck, U., "The Effect of Cu(II)-Loaded Brushite Scaffolds on Growth and Activity of Osteoblastic Cells," J. Biomed. Mater. Res. A, 100(9), 2012, pp. 2392–2400.

[118] Jackson, D. A., Smith, T. D., Amarsaikhan, N., Han, W., Neil, M. S., Boi, S. K., Vrabel, A. M., Tolosa, E. J., Almada, L. L., Fernandez-Zapico, M. E., and Elsawa, S. F., "Modulation of the IL-6 Receptor α Underlies GLI2-Mediated Regulation of Ig Secretion in Waldenström Macroglobulinemia Cells," J. Immunol. Baltim. Md 1950, 195(6), 2015, pp. 2908–2916.

[119] Clarke, B., "Normal Bone Anatomy and Physiology," Clin. J. Am. Soc. Nephrol. CJASN, 3(Suppl 3), 2008, pp. S131–S139.

[120] Ducheyne, P., Radin, S., and King, L., "The Effect of Calcium Phosphate Ceramic Composition and Structure on in Vitro Behavior. I. Dissolution," J. Biomed. Mater. Res., 27(1), 1993, pp. 25–34.

[121] Yoshida Katsumi, Hyuga Hideki, Kondo Naoki, Kita Hideki, Sasaki Miho, Mitamura Masanori, Hashimoto Kazuaki, and Toda Yoshitomo, "Substitution Model of Monovalent (Li, Na, and K), Divalent (Mg), and Trivalent (Al) Metal Ions for β-Tricalcium Phosphate," J. Am. Ceram. Soc., 89(2), 2005, pp. 688–690.

[122] Vahabzadeh, S., and Bose, S., "Effects of Iron on Physical and Mechanical Properties, and Osteoblast Cell Interaction in β-Tricalcium Phosphate," Ann. Biomed. Eng., 45(3), 2017, pp. 819–828.

[123] Bamberger, C. E., Specht, E. D., and Anovitz, L. M., "Crystalline Copper Phosphates: Synthesis and Thermal Stability," J. Am. Ceram. Soc., 80(12), 1997, pp. 3133–3138.

[124] Rath, S. N., Brandl, A., Hiller, D., Hoppe, A., Gbureck, U., Horch, R. E., Boccaccini, A. R., and Kneser, U., "Bioactive Copper-Doped Glass Scaffolds Can Stimulate Endothelial Cells in Co-Culture in Combination with Mesenchymal Stem Cells," PloS One, 9(12), 2014, p. e113319.

[125] Lin, Y., Xiao, W., Bal, B. S., and Rahaman, M. N., "Effect of Copper-Doped Silicate 13-93 Bioactive Glass Scaffolds on the Response of MC3T3-E1 Cells in Vitro and on Bone Regeneration and Angiogenesis in Rat Calvarial Defects in Vivo," Mater. Sci. Eng. C Mater. Biol. Appl., 67, 2016, pp. 440–452.

[126] Schamel, M., Bernhardt, A., Quade, M., Würkner, C., Gbureck, U., Moseke, C., Gelinsky, M., and Lode, A., "Cu2 +, Co2 + and Cr3 + Doping of a Calcium Phosphate Cement Influences Materials Properties and Response of Human Mesenchymal Stromal Cells," Mater. Sci. Eng. C, 73, 2017, pp. 99–110.

[127] O'Connor, E. M., and Durack, E., "Osteocalcin: The Extra-Skeletal Role of a Vitamin K-Dependent Protein in Glucose Metabolism," J. Nutr. Intermed. Metab., 7, 2017, pp. 8–13.

[128] Golub, E. E., and Boesze-Battaglia, K., "The Role of Alkaline Phosphatase in Mineralization," Curr. Opin. Orthop., 18(5), 2007, pp. 444–448.

[129] Ashammakhi, N., Reis, R. L., and Chiellini, E., *Topics in Tissue Engineering*, Oulu University, Oulu, Finland, 2007.

[130] Kong, Y. Y., Boyle, W. J., and Penninger, J. M., "Osteoprotegerin Ligand: A Common Link between Osteoclastogenesis, Lymph Node Formation and Lymphocyte Development," Immunol. Cell Biol., 77(2), 1999, pp. 188–193.

[131] Khairoun, I., Boltong, M. G., Driessens, F. C., and Planell, J. A., "Some Factors Controlling the Injectability of Calcium Phosphate Bone Cements," J. Mater. Sci. Mater. Med., 9(8), 1998, pp. 425–428.

[132] Xie, G., Sun, J., Zhong, G., Liu, C., and Wei, J., "Hydroxyapatite Nanoparticles as a Controlled-Release Carrier of BMP-2: Absorption and Release Kinetics in Vitro," J. Mater. Sci. Mater. Med., 21(6), 2010, pp. 1875–1880.

[133] Gaetke, L. M., and Chow, C. K., “Copper Toxicity, Oxidative Stress, and Antioxidant Nutrients,” Toxicology, 189(1–2), 2003, pp. 147–163.

[134] Kulanthaivel, S., Roy, B., Agarwal, T., Giri, S., Pramanik, K., Pal, K., Ray, S. S., Maiti, T. K., and Banerjee, I., “Cobalt Doped Proangiogenic Hydroxyapatite for Bone Tissue Engineering Application,” Mater. Sci. Eng. C, 58, 2016, pp. 648–658.

[135] Rath, S. N., Brandl, A., Hiller, D., Hoppe, A., Gbureck, U., Horch, R. E., Boccaccini, A. R., and Kneser, U., “Bioactive Copper-Doped Glass Scaffolds Can Stimulate Endothelial Cells in Co-Culture in Combination with Mesenchymal Stem Cells,” PLoS ONE, 9(12), 2014.

[136] Yang, L., Perez-Amodio, S., Barrère-de Groot, F. Y. F., Everts, V., van Blitterswijk, C. A., and Habibovic, P., “The Effects of Inorganic Additives to Calcium Phosphate on in Vitro Behavior of Osteoblasts and Osteoclasts,” Biomaterials, 31(11), 2010, pp. 2976–2989.

[137] Habibovic, P., and Barralet, J. E., “Bioinorganics and Biomaterials: Bone Repair,” Acta Biomater., 7(8), 2011, pp. 3013–3026.

[138] Lin, Y., Xiao, W., Bal, B. S., and Rahaman, M. N., “Effect of Copper-Doped Silicate 13-93 Bioactive Glass Scaffolds on the Response of MC3T3-E1 Cells in Vitro and on Bone Regeneration and Angiogenesis in Rat Calvarial Defects in Vivo,” Mater. Sci. Eng. C Mater. Biol. Appl., 67, 2016, pp. 440–452.

[139] Li, S., Xie, H., Li, S., and Kang, Y. J., “Copper Stimulates Growth of Human Umbilical Vein Endothelial Cells in a Vascular Endothelial Growth Factor-Independent Pathway,” Exp. Biol. Med. Maywood NJ, 237(1), 2012, pp. 77–82.

[140] Burghardt, I., Lüthen, F., Prinz, C., Kreikemeyer, B., Zietz, C., Neumann, H.-G., and Rychly, J., “A Dual Function of Copper in Designing Regenerative Implants,” Biomaterials, 44, 2015, pp. 36–44.

[141] Kulanthaivel, S., Mishra, U., Agarwal, T., Giri, S., Pal, K., Pramanik, K., and Banerjee, I., “Improving the Osteogenic and Angiogenic Properties of Synthetic Hydroxyapatite by Dual Doping of Bivalent Cobalt and Magnesium Ion,” Ceram. Int., 41(9, Part A), 2015, pp. 11323–11333.

[142] Zhang, M., Wu, C., Li, H., Yuen, J., Chang, J., and Xiao, Y., “Preparation, Characterization and in Vitro Angiogenic Capacity of Cobalt Substituted β-Tricalcium Phosphate Ceramics,” J. Mater. Chem., 22(40), 2012, pp. 21686–21694.

[143] Oh, R., and Brown, D. L., “Vitamin B12 Deficiency,” Am. Fam. Physician, 67(5), 2003, pp. 979–986.

[144] Yuan, Y., Hilliard, G., Ferguson, T., and Millhorn, D. E., “Cobalt Inhibits the Interaction Between Hypoxia-Inducible Factor-Alpha and von Hippel-Lindau Protein by Direct Binding to Hypoxia-Inducible Factor-Alpha,” J. Biol. Chem., 278(18), 2003, pp. 15911–15916.

[145] Balamurugan, K., “HIF-1 at the Crossroads of Hypoxia, Inflammation, and Cancer,” Int. J. Cancer, 138(5), 2016, pp. 1058–1066.

[146] Hirano, T., “Interleukin 6 (IL-6) and Its Receptor: Their Role in Plasma Cell Neoplasias,” Int. J. Cell Cloning, 9(3), 1991, pp. 166–184.

[147] Ghandadi, M., and Sahebkar, A., “Interleukin-6: A Critical Cytokine in Cancer Multidrug Resistance,” Curr. Pharm. Des., 22(5), 2016, pp. 518–526.

[148] Bravo, D., Shogren, K. L., Zuo, D., Wagner, E. R., Sarkar, G., Yaszemski, M. J., and Maran, A., “2-Methoxyestradiol-Mediated Induction of Frzb Contributes to Cell Death and Autophagy in MG63 Osteosarcoma Cells,” J. Cell. Biochem., 118(6), 2016, pp. 1497–1504.

[149] Kudina, O., Shogren, K. L., Gustafson, C. T., Yaszemski, M. J., Maran, A., and Voronov, A., “Invertible Micellar Polymer Nanoassemblies Target Bone Tumor Cells but Not Normal Osteoblast Cells,” Future Sci. OA, 1(3), 2015, p. FSO16.

[150] Bohner, M., “Reactivity of Calcium Phosphate Cements,” J. Mater. Chem., 17(38), 2007, pp. 3980–3986.

[151] Esposito, E., and Cuzzocrea, S., “TNF-Alpha as a Therapeutic Target in Inflammatory Diseases, Ischemia-Reperfusion Injury and Trauma,” Curr. Med. Chem., 16(24), 2009, pp. 3152–3167.

[152] Yasuyuki, M., Kunihiro, K., Kurissery, S., Kanavillil, N., Sato, Y., and Kikuchi, Y., “Antibacterial Properties of Nine Pure Metals: A Laboratory Study Using Staphylococcus Aureus and Escherichia Coli,” Biofouling, 26(7), 2010, pp. 851–858.

[153] Campbell, J. R., and Estey, M. P., “Metal Release from Hip Prostheses: Cobalt and Chromium Toxicity and the Role of the Clinical Laboratory,” Clin. Chem. Lab. Med., 51(1), 2013, pp. 213–220.

[154] Anissian, L., Stark, A., Dahlstrand, H., Granberg, B., Good, V., and Bucht, E., “Cobalt Ions Influence Proliferation and Function of Human Osteoblast-like Cells,” Acta Orthop. Scand., 73(3), 2002, pp. 369–374.

[155] Cheng, Y., Lin, C.-H., Chen, J.-Y., Li, C.-H., Liu, Y.-T., and Chen, B.-C., “Induction of Connective Tissue Growth Factor Expression by Hypoxia in Human Lung Fibroblasts via the MEKK1/MEK1/ERK1/GLI-1/GLI-2 and AP-1 Pathways,” PloS One, 11(8), 2016, p. e0160593.

[156] Nagao, H., Ijiri, K., Hirotsu, M., Ishidou, Y., Yamamoto, T., Nagano, S., Takizawa, T., Nakashima, K., Komiya, S., and Setoguchi, T., “Role of GLI2 in the Growth of Human Osteosarcoma,” J. Pathol., 224(2), 2011, pp. 169–179.

[157] Nagao-Kitamoto, H., Nagata, M., Nagano, S., Kitamoto, S., Ishidou, Y., Yamamoto, T., Nakamura, S., Tsuru, A., Abematsu, M., Fujimoto, Y., Yokouchi, M., Kitajima, S., Yoshioka, T., Maeda, S., Yonezawa, S., Komiya, S., and Setoguchi, T., “GLI2 Is a Novel Therapeutic Target for Metastasis of Osteosarcoma,” Int. J. Cancer, 136(6), 2015, pp. 1276–1284.

[158] Nagao-Kitamoto, H., Setoguchi, T., Kitamoto, S., Nakamura, S., Tsuru, A., Nagata, M., Nagano, S., Ishidou, Y., Yokouchi, M., Kitajima, S., Yoshioka, T., Maeda, S., Yonezawa, S., and Komiya, S., "Ribosomal Protein S3 Regulates GLI2-Mediated Osteosarcoma Invasion," Cancer Lett., 356(2 Pt B), 2015, pp. 855–861.

[159] Yang, W., Liu, X., Choy, E., Mankin, H., Hornicek, F. J., and Duan, Z., "Targeting Hedgehog-GLI-2 Pathway in Osteosarcoma," J. Orthop. Res. Off. Publ. Orthop. Res. Soc., 31(3), 2013, pp. 502–509.

[160] Mamlouk, S., and Wielockx, B., "Hypoxia-Inducible Factors as Key Regulators of Tumor Inflammation," Int. J. Cancer, 132(12), 2013, pp. 2721–2729.

[161] Biddlestone, J., Bandarra, D., and Rocha, S., "The Role of Hypoxia in Inflammatory Disease (Review)," Int. J. Mol. Med., 35(4), 2015, pp. 859–869.

[162] Elsawa, S. F., Almada, L. L., Ziesmer, S. C., Novak, A. J., Witzig, T. E., Ansell, S. M., and Fernandez-Zapico, M. E., "GLI2 Transcription Factor Mediates Cytokine Cross-Talk in the Tumor Microenvironment," J. Biol. Chem., 286(24), 2011, pp. 21524–21534.

[163] Mantovani, A., Allavena, P., Sica, A., and Balkwill, F., "Cancer-Related Inflammation," Nature, 454(7203), 2008, pp. 436–444.

[164] Noh, K., Kim, K.-O., Patel, N. R., Staples, J. R., Minematsu, H., Nair, K., and Lee, F. Y.-I., "Targeting Inflammatory Kinase as an Adjuvant Treatment for Osteosarcomas," J. Bone Joint Surg. Am., 93(8), 2011, pp. 723–732.